Dependence of diffusion in *Escherichia coli* cytoplasm on protein size, environmental conditions and cell growth

N. Bellotto[1], J. Agudo-Canalejo[2,†], R. Colin[1,†], R. Golestanian[2,3,+], G. Malengo[1,+], V. Sourjik[1,+]

[1]Max Planck Institute for Terrestrial Microbiology and LOEWE Center for Synthetic Microbiology (SYNMIKRO), Karl-von-Frisch-Strasse 16, D-35043 Marburg, Germany

[2]Max Planck Institute for Dynamics and Self-Organization, Am Faßberg 17, D-37077 Göttingen, Germany

[3]Rudolf Peierls Centre for Theoretical Physics, University of Oxford, Oxford OX1 3PU, United Kingdom

[†]These authors equally contributed to this work

[+]Corresponding authors: ramin.golestanian@ds.mpg.de, gabriele.malengo@synmikro.mpi-marburg.mpg.de, victor.sourjik@synmikro.mpi-marburg.mpg.de

Abstract

Inside prokaryotic cells, passive translational diffusion typically limits the rates with which cytoplasmic proteins can reach their locations. Diffusion is thus fundamental to most cellular processes, but the understanding of protein mobility in the highly crowded and non-homogeneous environment of a bacterial cell is still limited. Here we investigated the mobility of a large set of proteins in the cytoplasm of *Escherichia coli*, by employing fluorescence correlation spectroscopy (FCS) combined with simulations and theoretical modeling. We conclude that cytoplasmic protein mobility could be well described by Brownian diffusion in the confined geometry of the bacterial cell and at the high viscosity imposed by macromolecular crowding. We observed similar size dependence of protein diffusion for the majority of tested proteins, whether native or foreign to *E. coli*, and, for the faster-diffusing proteins, it is well consistent with the Stokes-Einstein relation once taking into account the specific dumbbell shape of protein fusions. Pronounced subdiffusion and hindered mobility are only observed for proteins with extensive interactions within the cytoplasm. Finally, while protein diffusion becomes markedly faster in actively growing cells, at high temperature, or upon treatment with rifampicin, and slower at high osmolarity, all of these perturbations affect proteins of different sizes in the same proportions, which could thus be described as changes of a well-defined cytoplasmic viscosity.

Introduction

Diffusion of molecules is important for the function of any cellular system, setting the upper limit for the mobility of proteins and other (macro)molecules and for the rates of many biochemical reactions that rely on random encounters between molecules (Schavemaker, Boersma, and Poolman 2018). Although the fundamental physics of diffusion in dilute aqueous solutions is well understood and mathematically described (Einstein 1906; Langevin 1908; Perrin 1909), diffusion in a cellular environment may be quite different (Schavemaker, Boersma, and Poolman 2018; Mika and Poolman 2011). The concentration of macromolecules in the bacterial cytoplasm, primarily proteins but also ribonucleic acids (RNAs), a phenomenon known as macromolecular crowding, is extremely high. For *Escherichia coli*, it is around 300 mg/mL, which corresponds to a volume fraction of 25-30% (Cayley et al. 1991; Zimmerman and Trach 1991). Such macromolecular crowding could hinder free diffusion and influence kinetics of protein association and of gene expression (Klumpp et al. 2013; Tabaka et al. 2014; van den Berg, Boersma, and Poolman 2017). The effects of crowding on protein diffusion have been demonstrated both *in vitro* and *in vivo* (Dix and Verkman 2008; Rivas and Minton 2016). Compared to water, the diffusion of a free green fluorescent protein (GFP) was reported to be three to four times slower in the eukaryotic cytoplasm (Swaminathan, Hoang, and Verkman 1997) and up to ten times slower in the bacterial cytoplasm (Elowitz Michael et al. 1999; Nenninger, Mastroianni, and Mullineaux 2010; Mika et al. 2010; Kumar, Mommer, and Sourjik 2010).

In addition to the high density of macromolecules, the diversity in the size and chemical properties of the solutes makes the cytoplasmic environment highly inhomogeneous (Luby-Phelps 1999; Spitzer and Poolman 2013). How much the diffusion of a particular molecule is affected by macromolecular crowding might thus depend on the size (Muramatsu and Minton 1988) and shape

of the molecule (Balbo et al. 2013) as well as on the nature of the crowders (Banks and Fradin 2005; Goins, Sanabria, and Waxham 2008). The effects of crowding observed in living cells appear to be even more complex, varying not only with the properties of the diffusing particle but also with the physiological state of the cell (Parry et al. 2014; Joyner et al. 2016) and the local cellular environment (Konopka et al. 2006; Persson, Ambati, and Brandman 2020). Moreover, non-trivial effects on diffusion arise due to reversible assembly and disassembly of the diffusing protein complexes (Agudo-Canalejo, Illien, and Golestanian 2020), and possibly also due to the active enhancement of enzyme diffusion by catalytic reactions (Golestanian 2015; Agudo-Canalejo et al. 2018; Zhang and Hess 2019).

The dependence of the diffusion coefficient (D) of a protein in the cytoplasm on its size might thus not necessarily follow the Stokes-Einstein (also called Stokes-Einstein-Sutherland-Smoluchowski) relation that is valid in dilute solutions, $D \propto T/(\eta R)$ (Einstein 1906), where T is the absolute temperature in Kelvin, η the viscosity of the medium and R the hydrodynamic radius of the particle. For globular proteins, R is given by the radius of gyration (Tyn and Gusek 1990) and depends on the molecular mass (MM) as $R \propto \mathrm{MM}^{\beta}$, where the exponent β would be 1/3 for perfectly compact and globular proteins but is in practice within the range of 0.35-0.43 for typical proteins, reflecting the fractal nature of the spatial distribution of protein mass (Smilgies and Folta-Stogniew 2015; Enright and Leitner 2005). Several studies of protein diffusion in the cytoplasm of *E. coli* have yielded different dependencies on the molecular mass, from ~0.33 (Nenninger, Mastroianni, and Mullineaux 2010) to ~2 (Kumar, Mommer, and Sourjik 2010), with an average β ~0.7 estimated based on the data pooled from multiple studies (Mika and Poolman 2011; Kalwarczyk, Tabaka, and Holyst 2012), and thus substantially steeper than predicted by the Stokes-Einstein relation. Similar exponent of ~0.7 was observed for limited sets of differently-sized proteins (Mika et al. 2010; Stracy et al. 2021). However, neither of these studies took explicitly into account the non-

77 globularity of the used fluorescent constructs, where two or more proteins are typically connected
78 by flexible linkers. For such multidomain proteins, shape fluctuations and hydrodynamic
79 interactions between the different domains can have a sizeable effect on the effective diffusion
80 coefficient of the whole protein (Agudo-Canalejo and Golestanian 2020), and they might thus be
81 important to consider when interpreting deviations from the Stokes-Einstein relation.

82 Besides macromolecular crowding, the translational diffusion of cytoplasmic proteins is also
83 influenced by intracellular structures, such as cytoskeletal filaments (Sabri et al. 2020), and by
84 (transient) binding to other macromolecules (Saxton 2007; Guigas and Weiss 2008; von Bülow et
85 al. 2019). Both these factors can not only reduce protein mobility but also lead to the anomalous
86 subdiffusive behavior, where the mean square displacement (MSD) of diffusing particles does not
87 scale linearly with time, as for Brownian diffusion in dilute solutions, but rather follows MSD $\propto t^{\alpha}$
88 with the anomalous diffusion exponent α being <1 (Saxton 1996; Etoc et al. 2018). Subdiffusion is
89 commonly observed in eukaryotes, particularly at longer spatial scales, primarily due to the
90 obstruction by the cytoskeletal filaments to the diffusion of proteins and larger particles (Di Rienzo
91 et al. 2014; Sabri et al. 2020). The mobility of larger nucleoprotein (Golding and Cox 2004; Lampo
92 et al. 2017) and multiprotein particles (Yu et al. 2018) in the bacterial cytoplasm is also
93 subdiffusive, while the diffusion of several tested small proteins was apparently Brownian (Bakshi,
94 Bratton, and Weisshaar 2011; English et al. 2011).

95 Even for the same protein, e.g. GFP or its spectral variants, estimates of the diffusion coefficient
96 in the cytoplasm obtained in different studies vary widely (Schavemaker, Boersma, and Poolman
97 2018), which could be in part due to differences in methodologies. Most early studies in bacteria
98 relied on fluorescence recovery after photobleaching (FRAP), where diffusion is quantified from
99 the recovery of fluorescence in a region of the cell bleached by a high intensity laser (Loren et al.

100 2015). These measurements provided values of diffusion coefficient for GFP ranging from 3 $\mu m^2 s^{-1}$
101 to 14 $\mu m^2 s^{-1}$ (Elowitz Michael et al. 1999; Mullineaux et al. 2006; Konopka et al. 2009; Kumar,
102 Mommer, and Sourjik 2010; Mika et al. 2010; Nenninger, Mastroianni, and Mullineaux 2010;
103 Schavemaker, Smigiel, and Poolman 2017). More recently, single-particle tracking (SPT), where
104 diffusion is measured by following the trajectories of single fluorescent molecules over time
105 (Kapanidis, Uphoff, and Stracy 2018), became increasingly used. Lastly, diffusion can also be
106 studied *in vivo* using fluorescence correlation spectroscopy (FCS) (Cluzel, Surette, and Leibler
107 2000), which measures the time required by a fluorescent molecule to cross the observation volume
108 of a confocal microscope (Elson 2011). SPT and FCS measure protein mobility locally within the
109 cell, with FCS having also a significantly better temporal resolution than FRAP and SPT. Both
110 methods provided higher but still varying values of D_{GFP}, from 8 $\mu m^2 s^{-1}$ up to 18 $\mu m^2 s^{-1}$ (Meacci
111 et al. 2006; English et al. 2011; Sanamrad et al. 2014; Diepold et al. 2017; Rocha et al. 2019).

112 Protein mobility also depends on the environmental and cellular conditions that affect the structure
113 of the bacterial cytoplasm (Schavemaker, Boersma, and Poolman 2018). Diffusion of large
114 cytoplasmic particles, measured by SPT, was shown to be sensitive to the antibiotics-induced
115 changes in the cytoplasmic crowding (Wlodarski et al. 2020) and to the energy-dependent
116 fluidization of the cytoplasm (Parry et al. 2014). Protein diffusion is also affected by high
117 osmolarity that increases macromolecular crowding and might create barriers to diffusion
118 (Konopka et al. 2006; Konopka et al. 2009; Liu et al. 2019). Furthermore, the surface charge of
119 cytoplasmic proteins has been shown to have a dramatic effect on their mobility (Schavemaker,
120 Smigiel, and Poolman 2017).

121 Variations between values of diffusion coefficients observed even for the same model organism in
122 different studies, each investigating only a limited number of protein probes, using different strains,

growth conditions and measurement techniques, hampered drawing general conclusions about the effective viscosity of bacterial cytoplasm and its dependence on the protein size. Furthermore, while the impact of several physiological perturbations on protein diffusion has been established, most of these previous studies used either large particles or free GFP, and how these perturbations affect properties of the cytoplasm over the entire physiological range of protein sizes remained unknown.

Here, we address these limitations by systematically analyzing the mobility of a large number of differently-sized cytoplasmic fluorescent protein constructs under standardized conditions by FCS. We further combined experiments with Brownian dynamics simulations and theoretical modeling of diffusion to correct for effects of confined cell geometry. Our work establishes general methodology to analyze FCS measurements of protein mobility in a confined space, which could be broadly applicable to cellular systems.

For the majority of studied constructs, we observe consistent dependence of the diffusion coefficient on the protein size, with a pronounced upper limit on diffusion at a given molecular mass. When corrected for the confinement due to the bacterial cell geometry, the diffusion of these constructs was nearly Brownian. Moreover, part of the deviation of the mass-dependence of their diffusion coefficients from the Stokes-Einstein relation might be explained by the specific shape of the fusion proteins. The slower and more anomalous diffusion of several protein constructs was apparently due to their strong interactions with other cellular proteins and protein complexes, and disruption of these interactions restored a Brownian diffusion close to the upper limit expected for their mass. Proteins that are not native to *E. coli* were observed to diffuse very similarly to their *E. coli* counterparts, except for their motion being slightly subdiffusive. Under the same experimental conditions FCS and FRAP measurements yield similar values of diffusion coefficients, suggesting

146 that no pronounced dependence of protein mobility on spatial scale could be observed in the
147 bacterial cytoplasm. Finally, we investigated the effects of environmental osmolarity and
148 temperature, of exposure to antibiotics and of cell growth on the mobility of proteins of different
149 size, demonstrating that the effects of all these perturbations, including cell growth, on protein
150 diffusion could be simply explained by changes in a unique cytoplasmic viscosity.

151

152 Results

153 Dependence of cytoplasmic protein mobility on molecular mass measured by 154 FCS

155 For our analysis of cytoplasmic protein mobility, we generated a plasmid-encoded library of 31
156 cytoplasmic proteins (Figure 1 – supplementary table 1 and supplementary table 2) of *E. coli* fused
157 to superfolder GFP (sfGFP) (Pédelacq et al. 2006). We selected proteins that, according to the
158 available information, are not known to bind DNA or to form homomultimers, although we did not
159 exclude *a priori* proteins that interact with other proteins. The structure of all selected proteins is
160 known and roughly globular, avoiding effects of the irregular protein shape on mobility. These
161 proteins belong to different cellular pathways. The expected size and stability of each construct
162 was verified by gel electrophoresis and immunoblotting (Figure 1 – figure supplement 1). Only
163 one of the constructs, ThpR-sfGFP, showed >20% degradation to free sfGFP, and it was therefore
164 excluded from further analyses. This was also the sole construct with an atypically high isoelectric
165 point (pI), and all remaining constructs have pI ranging from 5.1 to 6.2, as common for cytoplasmic
166 proteins (Schwartz, Ting, and King 2001). We further imaged the distribution of fusion proteins in
167 the cytoplasm. Except for RihA-sfGFP and NagD-sfGFP that were subsequently excluded, all other

168 constructs showed uniform localization (Figure 1A). Expression of most fusion proteins used for
169 the measurements of diffusion had little effect on *E. coli* growth (Figure 1 – figure supplement 2),
170 and even for several proteins that delayed the onset of the exponential growth, the growth rate
171 around the mid-log phase when cultures were harvested for the analysis was similar.
172 The mobility of the remaining 28 fusion constructs and of free sfGFP was investigated in living *E.*
173 *coli* cells by FCS (see Materials and Methods and Appendix 1). In order to reduce the impact of
174 photobleaching on FCS measurements, cell length was moderately (approximately twofold)
175 increased by treatment with the cell-division inhibitor cephalexin for 45 min, yielding an average
176 cell length of ~5 μm (Figure 1A). The resulting larger cell volume indeed reduces the rate of
177 photobleaching. During each FCS measurement, the laser focus was positioned close to the polar
178 region in the cell cytoplasm, in order to keep the confocal volume possibly away from both the cell
179 membrane and the nucleoid, and the fluorescence intensity in the confocal volume was measured
180 over time (Figure 1 – figure supplement 3). For each individual cell, six subsequent acquisitions of
181 20 s each were performed at the same position. The autocorrelation function (ACF) of the
182 fluorescence intensity fluctuations was independently calculated for each time interval and fitted
183 to extract the mobility parameters of the fluorescent proteins. Although we initially considered both
184 the Brownian diffusion and the anomalous diffusion models, the latter model proved to be
185 considerably better in fitting the experimental data (Figure 1 – figure supplement 4). The
186 anomalous diffusion model was therefore used to determine the diffusion (or residence) time (τ_D)
187 of a fluorescent molecule in the confocal volume and the anomalous diffusion exponent α for all
188 ACFs (Figure 1B and Figure 1 – supplementary table 1 and Figure 1 - figure supplement 3). The
189 averaged values of τ_D and α for each individual cell were then calculated from these six individual
190 acquisitions (Figure 1C and Figure 1 – figure supplement 5). Although, as mentioned above, all
191 finally used protein constructs showed no or little degradation, we tested a possible impact of the

192 fraction of free sfGFP for the construct that displayed the strongest (~15%) degradation, DsdA-
193 sfGFP. To this end, we fitted the FCS data using a model of two-components anomalous diffusion,
194 where the weight of the fast component was fixed to 15% and its values of τ_D and α to the average
195 values obtained for sfGFP (Figure 1 – figure supplement 6). The average value of τ_D for the slow
196 component was only ~7% lower compared to our regular fit using the one-component model, and
197 the value of α remained unchanged, suggesting that the impact of an even smaller fraction of free
198 GFP for other constructs could also be neglected.
199 Despite their substantial intercellular variability, the obtained mean values of the diffusion time
200 were clearly different between protein constructs (Figure 1C and Figure 1 – supplementary table
201 1). We next plotted the mean values of $1/\tau_D$, which reflect protein mobility, against the molecular
202 mass of protein constructs (Figure 1D). This dependence revealed a clear trend, where mobility of
203 more than half of the constructs decreased uniformly with their molecular mass, while some
204 exhibited much lower mobility than the other constructs of similar mass. In contrast, the anomalous
205 diffusion exponent α showed no apparent dependence on the protein size, ranging from 0.8 to 0.86
206 for most of the constructs (Figure 1E). Notably, the few protein constructs with α of ~ 0.8 or lower
207 were also among the ones with low mobility (Figure 1D and 1E, colored symbols). There was no
208 significant correlation between the values of $1/\tau_D$ or α and the length or the width of individual
209 cells, although a weak trend of α to increase with cell width might exist (Figure 1 – figure
210 supplement 7). Furthermore, no significant effect of the treatment with cephalexin for cells of
211 similar length (Figure 1 – figure supplement 8) could be observed.

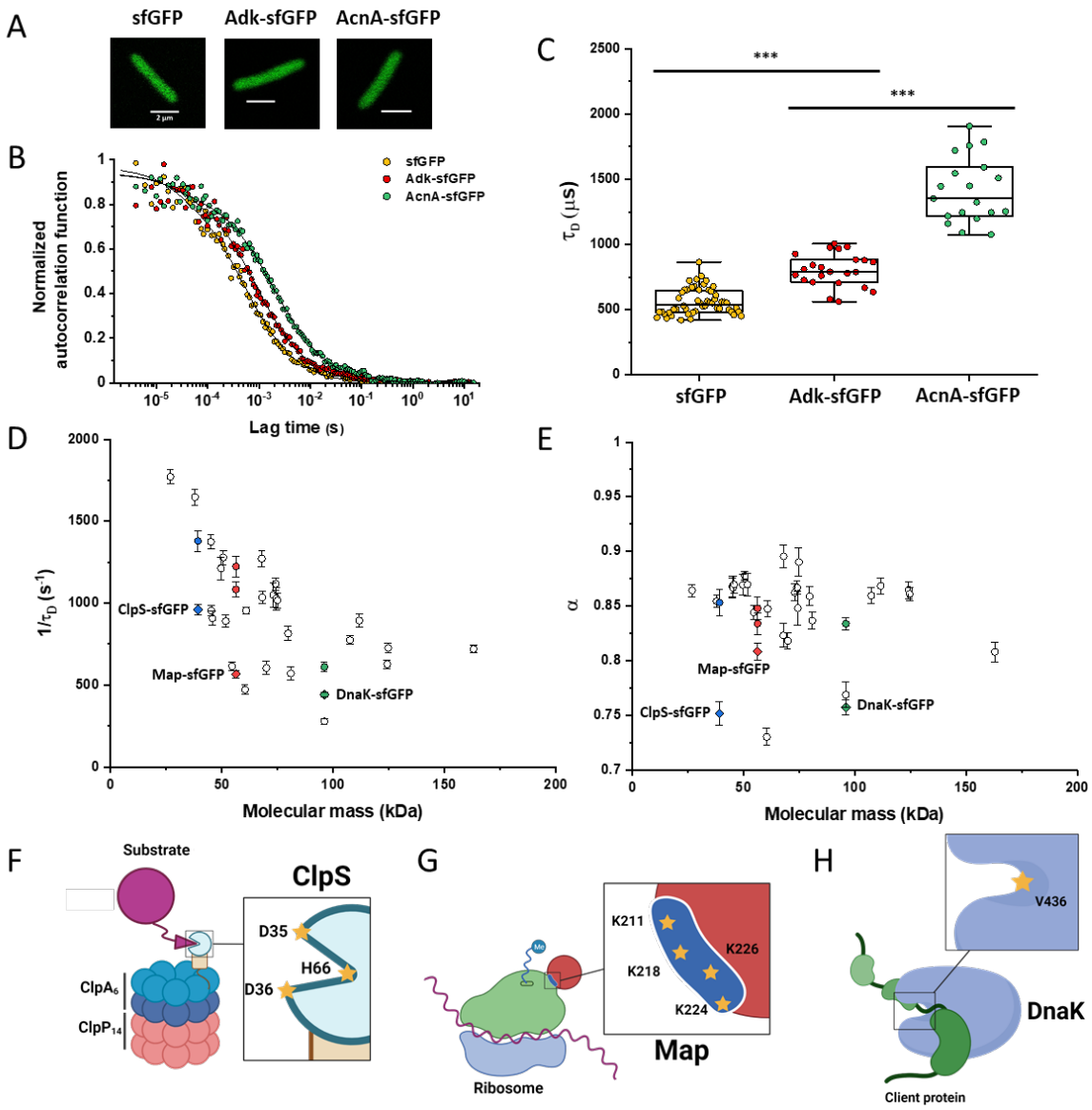

Figure 1. Dependence of protein mobility in bacterial cytoplasm on molecular mass and cellular interactions. (A) Examples of fluorescence microscopy images of *E. coli* cells expressing either sfGFP or the indicated sfGFP-tagged cytoplasmic proteins. Scale bar is 2 μm. (B) Representative autocorrelation functions (ACFs) measured by FCS for the indicated protein constructs. Data were fitted using the anomalous diffusion model (solid lines). All ACF curves were normalized to their respective maximal values to facilitate comparison. (C) Diffusion times (τ_D) measured for the indicated protein constructs. Each dot in the box plot represents the value for one individual cell, averaged over six consecutive acquisitions (Figure 1 – figure supplement 3) *** $p<0.0001$ in a two-tailed heteroscedastistic *t*-test. Exact p-values for all significance analyses performed in this study can be found in Appendix 4. (D, E). Dependence of protein mobility ($1/\tau_D$; D) and apparent anomaly of diffusion (α; E) on molecular mass. Each symbol represents the

222 average value for all individual cells that have been measured for that particular construct and the error bars represent
223 the standard error of the mean. Individual values are shown in Figure 1 – figure supplement 5 and the numbers of
224 measured cells for all the experiments performed in this study are shown in Appendix 5. Protein constructs with low
225 mobility for which effects of specific interactions were further investigated are highlighted in color and labeled. The
226 values of $1/\tau_D$ and α for both the original constructs (diamonds) and the constructs where mutations were introduced
227 to disrupt interactions (circles) are shown. For Map, two alternative amino acid substitutions that disrupt its interaction
228 with the ribosome are shown (see Figure 1 – figure supplement 10). (F-H) Cartoons illustrating the cellular interactions
229 that could affect mobility of ClpS (F), Map (G), and DnaK (H). ClpS engages with the ClpAP protease and with
230 substrates, cartoon adapted from (Roman-Hernandez et al. 2011). Map interacts with the actively translating ribosomes,
231 cartoon adapted from (Sandikci et al. 2013). DnaK interacts with unfolded client protein. Amino acidic residues that
232 were mutated to disrupt interactions are highlighted (see text for details).

233 **Figure 1 – source data**

234 Individual τ_D measurements from Figure 1C

235 Individual mean and standard errors of the mean of $1/\tau_D$ values from Figure 1D

236 Individual mean and standard errors of the mean of α values from Figure 1E

237

238 Macromolecular interactions reduce protein mobility

239 We reasoned that the main group of constructs that exhibit mobility close to the apparent mass-
240 dependent upper limit represents proteins whose diffusion is only limited by macromolecular
241 crowding, and that the lower $1/\tau_D$ and α of other constructs might be due to their specific
242 interactions with other cellular proteins or protein complexes. Indeed, for three of these proteins
243 (ClpS, Map, DnaK) such interactions are well characterized and can be specifically disrupted. ClpS
244 is the adaptor protein that delivers degradation substrates to the protease ClpAP (Roman-
245 Hernandez et al. 2011). The substrate-binding site of ClpS is constituted by three amino acid

246 residues (D35, D36, H66) that interact with the N-terminal degron of target proteins (Figure 1F).
247 If these residues are mutated into alanine, substrate binding *in vitro* is substantially reduced
248 (Roman-Hernandez et al. 2011; Humbard et al. 2013). Additionally, ClpS directly docks to the
249 hexameric ClpA. Consistently, we observed that while the stability of the mutant construct
250 $ClpS^{D35A_D36A_H66A}$-sfGFP was not affected (Figure 1 – figure supplement 9), its mobility in a *ΔclpA*
251 strain became significantly higher and less anomalous, with both $1/\tau_D$ and α reaching levels similar
252 to those of other proteins of similar mass (Figure 1D and 1E and Figure 1 – figure supplement 10).

253 Similar results were obtained for the other two constructs. Map is the methionine aminopeptidase
254 that cleaves the N-terminal methionine from nascent polypeptide chains (Solbiati et al. 1999). Map
255 interacts with the negatively charged backbone of ribosomes through four positively charged lysine
256 residues (K211, 218, 224, 226) located in a loop (Figure 1G). If these residues are mutated into
257 alanine, the *in vitro* affinity of Map for the ribosomes is reduced (Sandikci et al. 2013). The
258 mobility of Map-sfGFP was indeed much increased by alanine substitutions at all four lysine sites
259 (Figure 1D and 1E and Figure 1 – figure supplement 9 and figure supplement 10). Interestingly,
260 charge inversion of lysines to glutamic acid did not further increase Map-sfGFP mobility as was
261 expected based on *in vitro* experiments (Sandikci et al. 2013).

262 DnaK is the major bacterial chaperone that binds to short hydrophobic polypeptide sequences,
263 which become exposed during protein synthesis, membrane translocation or protein unfolding
264 (Genevaux, Georgopoulos, and Kelley 2007). DnaK accommodates its substrate peptides inside a
265 hydrophobic pocket (Figure 1H). The substitution of the valine residue 436 with bulkier
266 phenylalanine creates steric hindrance that markedly decreases substrate binding to DnaK *in vitro*
267 (Mayer, Rüdiger, and Bukau 2000), and both the $1/\tau_D$ and α of $DnaK^{V436F}$-sfGFP were significantly
268 higher than for the correspondent wild-type construct (Figure 1D and 1E and Figure 1 – figure

269 supplement 9 and figure supplement 10). Nevertheless, in this case the $1/\tau_D$ did not reach the levels
270 of other proteins of similar molecular mass, which is likely explained by multiple interactions of
271 DnaK with other components of the cellular protein quality control machinery besides its binding
272 to substrates (Kumar and Sourjik 2012).

273

274 Apparent anomaly of diffusion could be largely explained by confinement

275 When FCS measurements are performed in a confined space with dimensions comparable to those
276 of the observation volume, such confinement may affect the apparent mobility of fluorescent
277 molecules (Gennerich and Schild 2000; Jiang et al. 2020). To investigate the effect of confinement
278 on our FCS measurements, we performed Brownian dynamics simulations of FCS experiments
279 with particles undergoing three-dimensional, purely Brownian diffusion inside a bacterial cell-like
280 volume (Figure 2A *Inset*; see Materials and Methods). For the values of cell diameter commonly
281 observed under our growth conditions, 0.8-0.9 μm, and over a wide range of particle diffusion
282 coefficients, simulated autocorrelation functions could be indeed successfully fitted with the
283 anomalous diffusion model, yielding an anomalous diffusion exponent of around 0.8-0.9 (Figure
284 2A and 2B). This made us hypothesize that the relatively small apparent deviation from Brownian
285 diffusion in the fit, with α above 0.8 common to most constructs, may primarily reflect a
286 confinement-induced effect rather than proper subdiffusion.

287 In apparent agreement with these simulation results, when *E. coli* cell width was increased by
288 treatment with the inhibitor of bacterial cell wall biosynthesis A22 (Ouzounov et al. 2016) (Figure
289 2C), in addition to the standard cephalexin-induced elongation, the anomalous diffusion exponent
290 of sfGFP (Figure 2D) also significantly increased. A small, but significant increase in protein
291 mobility is also observed (Figure 2 – figure supplement 1). Since it was previously reported that

292 treatment with A22 can reduce dry-mass density of *E. coli* cells (Oldewurtel Enno, Kitahara, and
293 van Teeffelen 2021), we further performed a cell sedimentation assay (Figure 2 – figure supplement
294 2A-C). While the treatment with cephalexin slightly (by <0.1%) decreased the density of *E. coli*
295 cells in this assay, the additional treatment with A22, in our growth conditions, had only minor and
296 not significant impact once the effect of the volume increase on sedimentation was accounted for
297 (Figure 2 – figure supplement 2H). We thus conclude that the influence of A22 on the anomaly of
298 protein diffusion is most likely due to its effect on cell width and not on the cytoplasmic density.

299 To additionally test our conclusion that the reduced value of α is due to confinement by the cell
300 width, we performed FCS measurements for sfGFP and AcnA-sfGFP on a smaller confocal
301 volume, thus limiting the analysis to fluorophores diffusing at a distance from the cell boundary,
302 by reducing the pinhole size to a less optimal but smaller value of 0.66 Airy units. Indeed, the value
303 of α derived from these measurements was significantly higher for both proteins, >0.9 (Figure 2 -
304 figure supplement 3A), consistent with our prediction. As expected, the residence time (τ_D) of
305 proteins in such a smaller confocal volume is also smaller (Figure 2 - figure supplement 3B)

306 We next derived an Ornstein-Uhlenbeck (OU) model for fitting FCS data, where the confinement
307 of Brownian diffusing fluorescent particles within the width of the cell is approximated by trapping
308 in a harmonic potential of the same width (Appendix 2). The two models fit the ACF of the
309 Brownian dynamic simulations comparably well and better than the model of unconfined Brownian
310 diffusion (Figure 2A and Figure 2 - figure supplement 4), with the OU model having one less free
311 parameter than the anomalous diffusion model. The OU model directly estimates the ansatz
312 diffusion coefficient with ± 5% accuracy for the typical cell widths observed in our experiments
313 (Figure 2 – figure supplement 5).

314 Since the OU model proved accurate in fitting the experimental data, comparably to the anomalous
315 diffusion model (Figure 2 – figure supplement 6), we used it to re-fit the ACF data for all faster
316 diffusing constructs and to estimate their Brownian diffusion coefficients (Figure 2E and Figure 1
317 – supplementary table 1). The dependence of D on molecular mass for this set of constructs was
318 scaling as $(MM)^{-\beta}$ with $\beta = 0.56 \pm 0.05$ (Figure 2F, solid blue line), less steep compared to the
319 previous estimates (Kumar, Mommer, and Sourjik 2010; Mika et al. 2010; Stracy et al. 2021) but
320 still steeper than expected from the Stokes-Einstein relation, even when assuming $\beta = 0.4$ for not
321 perfectly globular proteins (Figure 2F, black dashed line) (Enright and Leitner 2005; Smilgies and
322 Folta-Stogniew 2015). In order to elucidate whether part of this residual deviation may be
323 accounted for by the specific shape of fusion constructs, where sfGFP is fused to the differently-
324 sized target proteins by a short flexible linker, we further applied a previously derived model
325 describing diffusion of such linked proteins (Appendix 3) (Agudo-Canalejo and Golestanian 2020).
326 The dependence of D on molecular mass predicted by this linked-protein model seems indeed to
327 better recapitulate our experimental data, particularly for smaller protein fusions (Figure 2F, solid
328 yellow line), although it moderately overestimates D for several of the largest protein fusions (>100
329 kDa). Thus, we conclude that the size dependence of diffusion for the majority of cytoplasmic
330 proteins follows the Stokes-Einstein relation, once the shape of the sfGFP-tagged protein constructs
331 is taken into account.

332

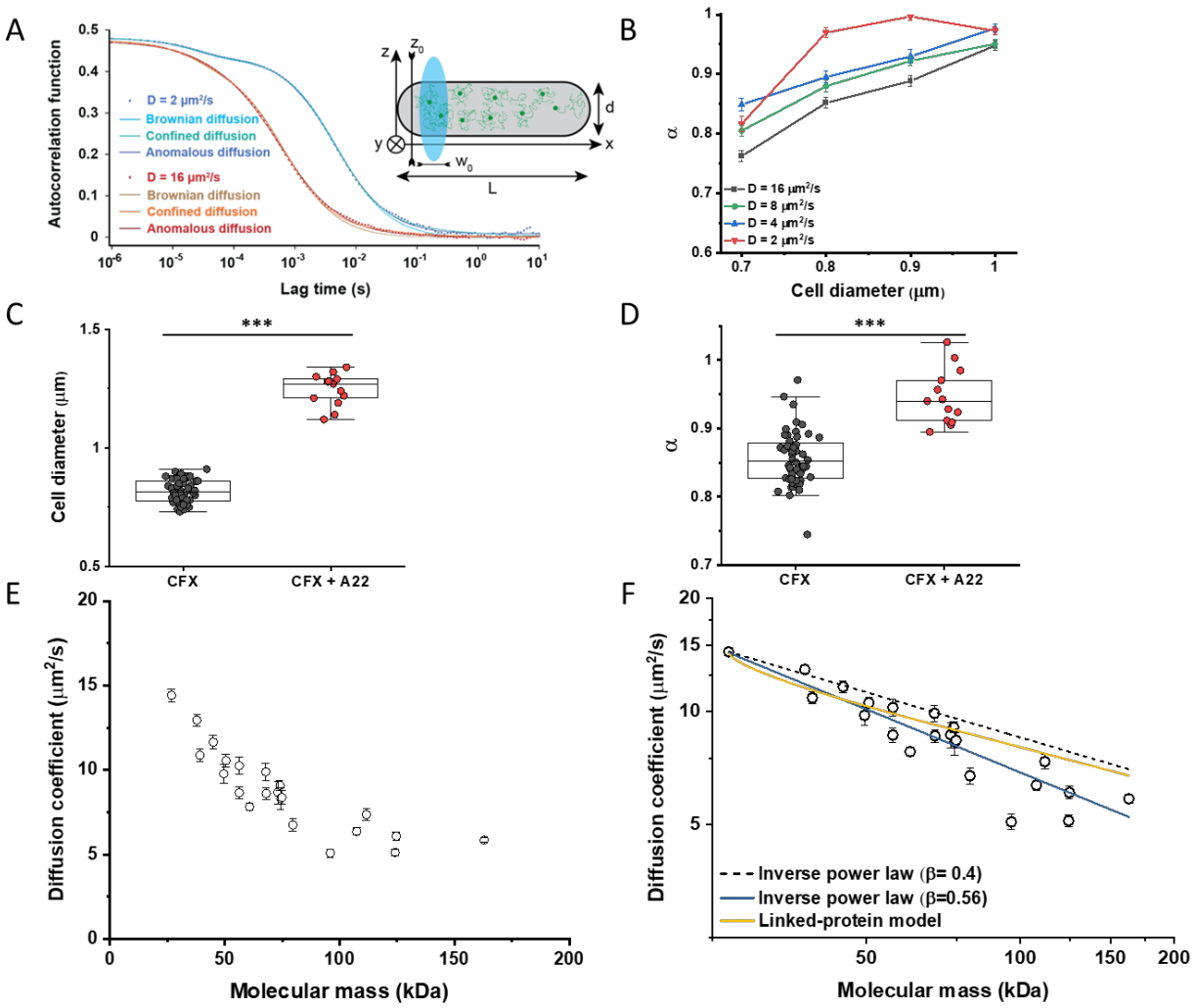

Figure 2. Protein diffusion in bacterial cytoplasm corrected for confinement. (A) Representative ACFs of simulated fluorescence intensity fluctuations. Simulations were performed in a confined geometry of a cell with indicated length L and diameter d, and dimensions of the measurement volume ω_0 and z_0, representing an experimental FCS measurement (*Inset*; see Materials and Methods) for two different values of the ansatz diffusion coefficient. Solid lines are fits by the models of unconfined Brownian diffusion, anomalous diffusion and by the Ornstein-Uhlenbeck (OU) model of Brownian diffusion under confinement, as indicated. (B) The exponent α extracted from the fit of the anomalous diffusion model to the ACFs data that were simulated at different values of the cell diameter. Corresponding values of the diffusion coefficient are shown in Figure 2 – figure supplement 5. (C, D) *E. coli* cells treated with cephalexin alone or with cephalexin and 1 μg/mL of A22 (see Materials and methods), show A22-dependent increase in the measured cell diameter (C) and higher values of the exponent α extracted from the fit to the ACF measurements (D). *** $p<0.0001$ in a two-tailed heteroscedastistic *t*-test. (E) Dependence of the diffusion coefficient calculated from

345 fitting the experimental ACFs with the OU model of confined diffusion. Only the subset of apparently freely diffusing
346 constructs from Figure 1D has been analyzed with the OU model (see also Figure 1 – supplementary table 1). Each
347 circle represents the average value for all individual cells that have been measured for that particular construct
348 (Appendix 5), and the error bars represent the standard error of the mean. Error bars that are not visible are smaller
349 than the symbol size. (F) Fit of the mass dependence with an inverse power law (solid blue line, exponent $\beta = 0.56 \pm$
350 0.05), and predictions of the Stokes-Einstein relation (black dashed line) and of the model describing diffusion of two
351 linked globular proteins (solid yellow line), both with exponent $\beta = 0.4$.

352 **Figure 2 – source data**

353 Average and error from each simulation in Figure 2B

354 Individual measurements of cell diameters from Figure 2C

355 Individual measurements of α from Figure 2D

356 Individual mean and standard error of the mean of diffusion coefficient values from Figure 2E and 2F

357

358 Protein diffusion coefficients measured using FRAP or FCS are consistent

359 Since many previous measurements of protein diffusion in bacteria were performed using FRAP,
360 we aimed to directly compare the results of FRAP and FCS measurements for a set of constructs
361 of different mass. Importantly, we used the same growth conditions and microscopy sample
362 preparation protocols as for the FCS experiments. The cells were photobleached in a region close
363 to the pole, similar to the position that was used for the FCS experiment. The recovery of
364 fluorescence was then followed for 11 seconds with the time resolution of 18 ms (Figure 3A). The
365 diffusion coefficients were computed from the time course of recovery with the plugin for ImageJ,
366 simFRAP (Blumenthal et al. 2015), which utilizes a simulation-based approach (Figure 3B). We
367 observed very good correlation between both values of diffusion coefficients, although for most

368 constructs the diffusion coefficients determined by FRAP were 5 to 30% lower than those obtained

369 from the FCS data (Figure 3C and Figure 1 – supplementary table 1).

370

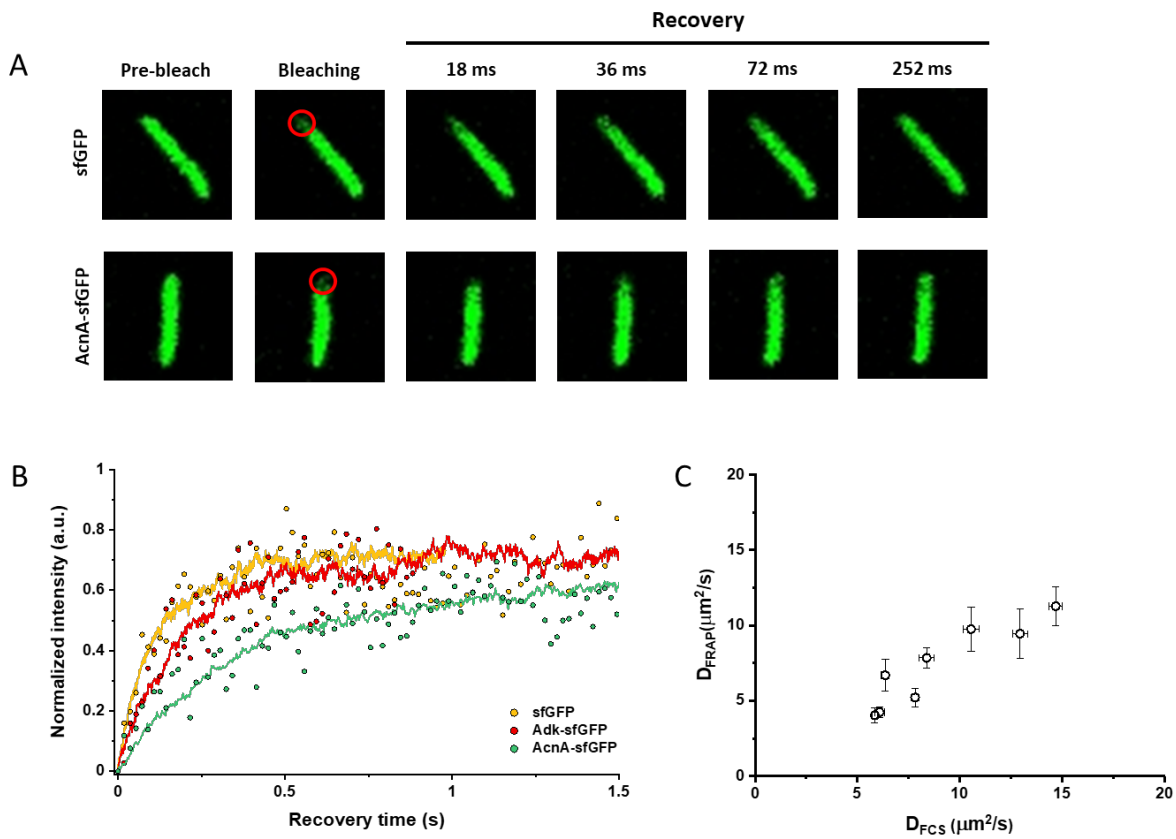

371

372 **Figure 3. Comparison between protein diffusion coefficients measured by FCS and FRAP.** (A) Examples of

373 FRAP measurements for two different constructs, sfGFP and AcnA-sfGFP. A 3x3 pixels area close to one cell pole

374 (red circle) was photobleached with a high intensity laser illumination for 48 ms and the recovery of fluorescence in

375 the bleached area was monitored for 11 s with the time resolution of 18 ms. (B) Representative curves of fluorescence

376 recovery in FRAP experiments and their fitting using simFRAP. The experimental data (colored dots) are used by the

377 simFRAP algorithm to simulate the underlying diffusional process (colored lines). The simulation is then used to

378 compute the diffusion coefficient. The simulation proceeds until the recovery curve reaches a plateau, therefore it is

379 interrupted at a different time for each curve. (C) Correlation between the diffusion coefficients measured in FCS

380 experiments (D_{FCS}, fitting with the OU model; data from Figure 2E) and in FRAP experiment (D_{FRAP}, fitting with

381 simFRAP). Error bars represent the standard error of the mean. Error bars that are not visible are smaller than the
382 symbol size.

383 **Figure 3 – source data**

384 Individual mean and standard error of the mean of diffusion coefficient values from Figure 3C

385

386 Diffusive properties of cytoplasmic proteins are largely conserved between 387 bacterial species

388 We then investigated whether sfGFP fusions to non-native proteins, originating from other bacteria,
389 may show different diffusive properties in *E. coli* cytoplasm than their native counterparts. The
390 existence of an organism-dependent "quinary" code of unspecific, short living interactions has been
391 recently proposed in order to explain the reduced mobility of heterologous human proteins in *E.*
392 *coli* cytoplasm (Mu et al. 2017). Thus, we investigated the mobility of proteins from other Gram-
393 negative proteobacteria *Yersinia enterocolitica*, *Vibrio cholerae*, *Caulobacter crescentus* and
394 *Myxococcus xanthus* and from the Gram-positive bacterium *Bacillus subtilis* that are homologous
395 to several analyzed freely-diffusing *E. coli* protein constructs. Within this set of constructs, we
396 observed no significant differences of their $1/\tau_D$ values from *E. coli* homologues. An exception was
397 AcnA from *M. xanthus* (Figure 4A and Figure 4 – figure supplement 1A), whose lower mobility
398 might be a sign of its multimerization, although cellular distribution of this construct was uniform.
399 In contrast, all constructs showed slightly but mostly significantly increased anomaly of diffusion
400 compared to *E. coli* proteins (Figure 4B and Figure 4 – figure supplement 4B), which might reflect
401 the weakly increased propensity of non-native proteins to engage in unspecific interactions in *E.*
402 *coli* cytoplasm.

403

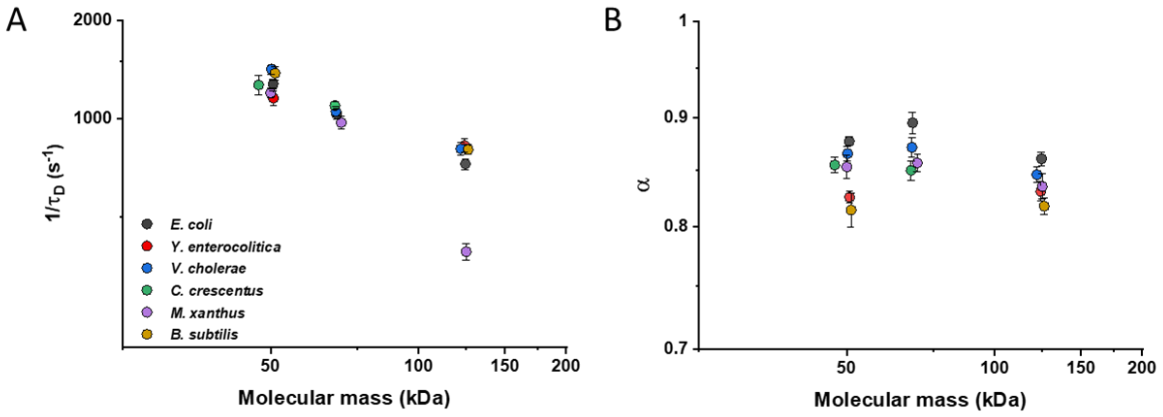

Figure 4. Mobility of homologous proteins from other bacterial species in *E. coli*. Mass dependence of protein mobility ($1/\tau_D$; A) and anomaly of diffusion (α; B) of sfGFP fusions to homologues of Adk, Pgk and AcnA from indicated bacterial species (*E.c. = Escherichia coli; Y.e. = Yersinia enterocolitica; V.c. = Vibrio cholerae; C.c. = Caulobacter crescentus; M.x. = Myxococcus xanthus; B.s. = Bacillus subtilis*) compared with that of their counterpart from *E. coli*. Each symbol represents the average value for all individual cells that have been measured for that construct (Appendix 5) and the error bars represent the standard error of the mean. Error bars that are not visible are smaller than the symbol size.

Figure 4 – source data

Individual mean and standard error of the mean of $1/\tau_D$ values from Figure 4A

Individual mean and standard error of the mean of α values from Figure 4B

Effects of osmolarity, temperature, antibiotics and cell growth on mobility of differently-sized proteins

We further characterized the impact of several environmental and cellular perturbations of the bacterial cytoplasm on protein mobility, using apparently freely diffusing protein fusions of

421 different sizes as probes. We started with the previously characterized decrease in mobility of GFP
422 and large protein complexes or aggregates upon osmotic upshift (Konopka et al. 2006; Konopka et
423 al. 2009; Mika et al. 2010; Liu et al. 2019; Wlodarski et al. 2020). *E. coli* cells exposed to increased
424 ionic strength by addition of 100 mM NaCl showed decrease in cell length and width (Figure 5 –
425 figure supplement 1A, B) and an increase in cell density in the sedimentation assay (Figure 2 –
426 figure supplement 2D), consistent with a previous report (Wlodarski et al. 2020). Higher ionic
427 strength also significantly decreased the mobility of sfGFP (Figure 5A and Figure 5 – figure
428 supplement 2A), comparably to previously measured values (Konopka et al. 2009; Mika et al.
429 2010). Importantly, the mobility of all other tested constructs decreased proportionally (Figure 5A),
430 meaning that – in this range of molecular sizes – the effect of a moderate osmotic upshift can be
431 interpreted as a simple increase in cytoplasmic viscosity due to higher molecular crowding, which
432 is in contrast to the different effects of high osmolarity on small molecules and on GFP (Mika et
433 al. 2010). No effect is observed on the anomaly of diffusion for any protein construct (Figure 5 –
434 figure supplement 3A).

435 Next, we studied the effect of environmental temperature on protein mobility in bacterial
436 cytoplasm. According to the Stokes-Einstein equation, the diffusion of a particle directly depends
437 on the system's temperature in Kelvin and on the viscosity of the fluid, which itself changes with
438 temperature. In the biologically relevant range, the temperature sensitivity of diffusion is primarily
439 determined by the temperature dependence of water viscosity. The measured increase in mobility
440 of sfGFP and two other constructs, by approximately 20-25% between 25°C and 35°C (Figure 5B
441 and Figure 5 – figure supplement 2B), agrees well with the temperature-dependent decrease in
442 water viscosity over 10°C (Huber et al. 2009). Expectedly, the effect of imaging temperature was
443 not linked to any changes of the cell size (Figure 5 – figure supplement 1C, D). Of note, a weak,
444 but consistent, increase in the anomaly of protein diffusion is also observed at higher environmental

445 temperature (Figure 5 – figure supplement 3B). Instead, the growth temperature of the *E. coli*
446 culture had no apparent effect on protein mobility (Figure 5 – figure supplement 4), suggesting that
447 – at least in the tested temperature range – *E. coli* lacks the growth-temperature dependent
448 regulation of cytoplasmic viscosity that has been recently reported in the budding yeast (Persson,
449 Ambati, and Brandman 2020).

450 Antibiotics that inhibit transcription (e.g., rifampicin) or translation (e.g., chloramphenicol) are
451 known to affect the spatial organization of bacterial chromosomes (Bakshi et al. 2014). The
452 mobility of chromosomal loci and of large cytoplasmic aggregates was also shown to be affected
453 by several antibiotics, in apparent correlation with changes in the cytoplasmic density (Wlodarski
454 et al. 2020). We observed that chloramphenicol treatment caused a minor increase in cell width
455 (Figure 5 – figure supplement 1F) and a decrease in cell density (Figure 2 – figure supplement 2G).
456 However, protein mobility rather decreased in chloramphenicol-treated cells, opposite to what
457 could be expected based alone on the chloramphenicol-induced reduction of cell density (Figure
458 5C and Figure 5 – figure supplement 2C). The reduced protein mobility could neither be simply
459 explained by compaction of the nucleoid in cells treated with chloramphenicol, since it was only
460 marginally lower inside than outside of the nucleoid (Figure 5 – figure supplement 5A, B). It should
461 be noted that no significant difference in the anomaly of diffusion (Figure 5 – figure supplement
462 5C) was observed inside or outside of the nucleoid.

463 In contrast, inhibition of RNA transcription by rifampicin treatment led to a marked increase in
464 protein mobility (Figure 5C and Figure 5 – figure supplement 2C). Such higher protein mobility is
465 consistent with the previously observed rifampicin-induced reduction of macromolecular crowding
466 in bacterial cytoplasm (Wlodarski et al. 2020), although only a minor decrease in cell density was
467 observed in our sedimentation assay (Figure 2 – figure supplement 2F) beyond the effect of DMSO

468 that was used as a solvent for rifampicin (Figure 2 – figure supplement 2E). Similar to the effects
469 of osmolarity and temperature, the increase in protein mobility caused by the rifampicin treatment,
470 and its decrease induced by chloramphenicol were similar for all tested proteins (Figure 5C), except
471 for the AcnA-sfGFP construct that was disproportionally affected by chloramphenicol in both
472 mobility and anomaly of diffusion (Figure 5 – figure supplement 3C).

473 Finally, we investigated whether protein mobility might be influenced by cell growth, comparing
474 FCS measurements in cells incubated at 35°C on agarose pads containing either only M9 salts or
475 M9 salts plus glucose and casamino acids. These conditions had only minor impact on the cell
476 shape (Figure 5 – figure supplement 1G, H). Although at this high temperature residual growth was
477 also observed for cells on M9 salt pads, cell growth in presence of nutrients was expectedly much
478 more pronounced. The observed protein mobility was also much higher in the presence of nutrients,
479 and this increase was again similar for the four tested differently-sized constructs (Figure 5D and
480 Figure 5 – figure supplement 2D), while no consistent trend was observed in the anomaly of protein
481 diffusion across these conditions (Figure 5 – figure supplement 3D). To further distinguish the
482 respective contributions of metabolic activity and of biosynthesis and resulting cell growth, we
483 incubated cells in presence of both nutrients and chloramphenicol on the agarose pad. Similar to
484 our previous experiments where chloramphenicol was added to the batch culture, its addition had
485 no or little effect on the mobility of sfGFP or the AcnA-sfGFP construct in absence of nutrients
486 (Figure 5 – figure supplement 6). In contrast, protein mobility in presence of nutrients was strongly
487 affected by chloramphenicol treatment. Thus, the enhanced protein mobility in presence of
488 nutrients appears to be primarily due to active protein production and cell growth. Nevertheless,
489 even chloramphenicol-treated cells exhibited a moderate increase in protein mobility in presence
490 of nutrients, indicating that the metabolic activity contributes to the overall effect of growth on

491 diffusion. It is possible that the contribution of the metabolic activity might be even larger than it
492 appears in this experiment, since the inhibition of protein translation might reduce metabolic
493 activity. In any case, the impact of growth on diffusion of individual proteins cannot be simply
494 explained by the energy state of the cell, since lowering it by the inhibition of respiration-dependent
495 ATP synthesis using treatment with dinitrophenol (DNP) did not reduce protein mobility, at either
496 25°C or 35°C. This is contrary to the effect of the DNP treatment on large cytoplasmic particles
497 (Parry et al. 2014) (Figure 5– figure supplement 7). An interesting exception was the mobility of
498 Adk-sfGFP, which was indeed reduced by the DNP treatment at high temperature. This, however,
499 might be a specific effect related to the enzymatic activity or conformation of Adk that binds ATP
500 as a substrate.

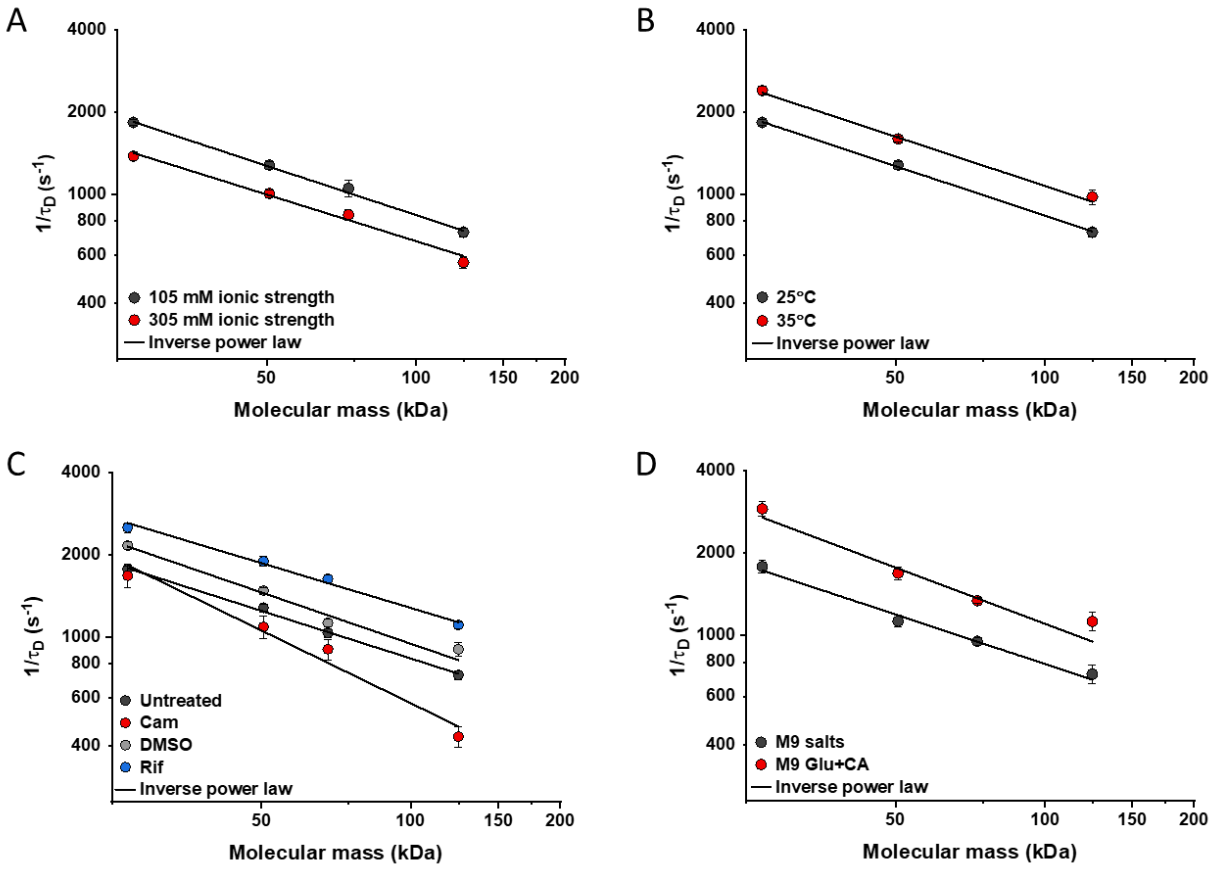

501

502 **Figure 5. Effects of physicochemical perturbations and cell growth on mobility of differently-sized proteins.**
503 Each dot represents the average value of protein mobility ($1/\tau_D$) of all the cells measured for the construct of the
504 indicated molecular mass (Appendix 5). Error bars represent the standard error. Error bars that are not visible are
505 smaller than the symbol size. The solid black lines are the fit with an inverse power law to extract the size dependence
506 of protein mobility (β) in that condition. (A) Protein mobility measured in cells that were resuspended in either
507 tethering buffer (ionic strength of 105 mM; $\beta = 0.60 \pm 0.01$) or in the same buffer but supplemented with additional
508 100 mM NaCl (total ionic strength of 305 mM; $\beta = 0.57 \pm 0.05$). The measurements were performed in agarose pads
509 prepared at the same ionic strength. (B) Protein mobility at different environmental temperatures. As for the other
510 experiments, *E. coli* cultures were grown at 37°C and bacterial cells during the measurements were incubated at 25°C
511 ($\beta = 0.60 \pm 0.01$) or at 35°C ($\beta = 0.60 \pm 0.05$), as indicated. (C) Protein mobility in control cells ($\beta = 0.58 \pm 0.02$) and
512 after treatment with chloramphenicol (Cam; 200 µg/mL; $\beta = 0.88 \pm 0.11$), rifampicin (Rif; 200 µg/mL, in 0.1% v/v
513 DMSO; $\beta = 0.54 \pm 0.04$), or DMSO control (0.1% v/v; $\beta = 0.62 \pm 0.07$) as indicated. Antibiotics were added to growing
514 *E. coli* culture 60 minutes prior to harvesting. (D) Protein mobility in non-growing cells incubated at 35°C on agarose
515 pads containing only M9 salts ($\beta = 0.60 \pm 0.05$) in comparison with growing cell incubated on pads with M9 salts
516 supplemented with 20 mM glucose and 0.2% casamino acids (Glu + CA; $\beta = 0.68 \pm 0.10$).

517 **Figure 5 – source data**

518 Individual mean and standard error of the mean of $1/\tau_D$ values from Figure 5A

519 Individual mean and standard error of the mean of $1/\tau_D$ values from Figure 5B

520 Individual mean and standard error of the mean of $1/\tau_D$ values from Figure 5C

521 Individual mean and standard error of the mean of $1/\tau_D$ values from Figure 5D

522

523 # Discussion

524 Bacteria rely on translational diffusion to deliver proteins and other macromolecules to their
525 cellular destinations, including their reaction partners, and the diffusional properties of bacterial
526 cytoplasm are therefore fundamental to the understanding of bacterial cell biology. Consequently,
527 a number of studies have investigated protein mobility in bacteria, all showing strong effects of
528 macromolecular crowding in the bacterial cytoplasm on diffusion (Konopka et al. 2006;
529 Mullineaux et al. 2006; Konopka et al. 2009; Kumar, Mommer, and Sourjik 2010; Mika et al. 2010;
530 Nenninger, Mastroianni, and Mullineaux 2010). Nevertheless, the relatively small number of
531 proteins investigated in each of these previous studies, and the differences between strains, growth
532 conditions and between methodologies, limited general conclusions about protein mobility, even
533 in the most-studied environment of *E. coli* cytoplasm. For example, combining data from different
534 studies to determine the relation between the size of a protein and its cytoplasmic diffusion
535 coefficient yielded only uncertain estimates (Mika and Poolman 2011; Schavemaker, Boersma,
536 and Poolman 2018). Such variability between different studies might be further compounded by
537 potentially profound effects on diffusion of size-independent protein properties such as surface
538 charge (Schavemaker, Smigiel, and Poolman 2017) or weak interactions with other proteins and
539 other cellular components (von Bülow et al. 2019). Similarly, it remains unclear whether a typical
540 protein in the cytoplasm exhibits Brownian diffusion, as has been shown in few examples (Bakshi,
541 Bratton, and Weisshaar 2011; English et al. 2011), or rather a subdiffusive behavior as common in
542 eukaryotic cells (Di Rienzo et al. 2014; Sabri et al. 2020) and for large proteins and nucleoprotein
543 particles in bacteria (Golding and Cox 2004; Lampo et al. 2017; Yu et al. 2018). Additionally,
544 while in eukaryotic cells anomalous diffusion is primarily associated with hindrance by
545 intracellular structures, the possible causes of anomalous diffusion in bacteria are still unclear.

546 Here, we addressed these questions by systematically investigating the diffusive behavior of a large
547 set of fluorescent protein fusions to differently-sized cytoplasmic proteins of *E. coli*. We

548 demonstrate that the majority of studied proteins exhibit a rather uniform relation between their
549 molecular mass and cytoplasmic mobility, with a clear upper bound on protein mobility at a given
550 molecular mass. This bound likely reflects the fundamental size-specific physical limit on protein
551 diffusion in *E. coli* cytoplasm, with lower mobility of individual proteins being due to their
552 interactions with other cellular components.

553 Furthermore, our simulations suggest that the apparent weak anomaly of diffusion observed in the
554 FCS data analysis, with $\alpha \sim 0.85$-0.9 for most proteins, could be accounted for by confinement of
555 the otherwise purely Brownian diffusing particles in the small volume of a bacterial cell. Similar
556 conclusions have been drawn by previous SPT studies for several individual proteins (Bakshi,
557 Bratton, and Weisshaar 2011; English et al. 2011). This interpretation is consistent with our
558 measurements of diffusion in A22-treated *E. coli* with an increased cell. Although the interpretation
559 of these experiments might be complicated by the reduced cytoplasmic density of A22-treated
560 bacteria (Oldewurtel Enno, Kitahara, and van Teeffelen 2021), under our conditions the effect of
561 A22 on cell density seems to be negligible. It is also supported by the FCS measurements using
562 smaller confocal volume, which yielded higher value of α, as could be expected from protein
563 diffusion away from the cell boundary.

564 We therefore used a model of purely Brownian diffusion under confinement (Ornstein-Uhlenbeck
565 model) to determine diffusion coefficients by directly fitting the autocorrelation functions of our
566 FCS measurements. The obtained overall dependence of diffusion coefficients on the molecular
567 mass of the fusion protein showed the exponent $\beta = 0.56$, steeper than predicted by the Stokes-
568 Einstein relation, with $\beta = 0.33$ for fully compact proteins or $\beta = 0.4$ for the more realistic case
569 where proteins are assumed to be not entirely compact (Enright and Leitner 2005; Smilgies and
570 Folta-Stogniew 2015). Nevertheless, at least for smaller constructs, the observed dependence of

571 the diffusion coefficient on the molecular mass could be well reproduced once the specific shape
572 of fusion constructs, where two roughly globular proteins are fused by a short linker, was taken
573 into account along with their imperfect globularity (Agudo-Canalejo and Golestanian 2020). Only
574 largest proteins in our set (above 100 kDa) showed mobility that was slower than predicted by this
575 model, possibly because diffusion of larger proteins is more strongly impacted by weak interactions
576 with other macromolecules (von Bülow et al. 2019).

577 Our analysis thus suggests that, despite the high crowdedness of the bacterial cytoplasm, the
578 diffusion of typical cytoplasmic proteins in bacteria is mostly Brownian and can be well described
579 by treating the cytoplasm as a viscous fluid, with only a moderate dependence of the effective
580 viscosity on the size of diffusing proteins. Given the diffusion coefficient determined in our study
581 for free sfGFP, ~14 $\mu m^2 s^{-1}$, for small proteins this effective viscosity of bacterial cytoplasm is only
582 approximately six times higher than in dilute solution (Potma et al. 2001). This diffusion coefficient
583 for GFP is substantially larger than the values reported in the early studies that used FRAP (Elowitz
584 Michael et al. 1999; Konopka et al. 2006; Mullineaux et al. 2006; Konopka et al. 2009; Kumar,
585 Mommer, and Sourjik 2010; Mika et al. 2010; Nenninger, Mastroianni, and Mullineaux 2010),
586 although it is consistent with other FCS and SPT studies (Meacci et al. 2006; English et al. 2011;
587 Sanamrad et al. 2014; Diepold et al. 2017; Rocha et al. 2019). These differences are apparently due
588 to the limitations of early FRAP analyses that generally underestimated protein mobility, rather
589 than due to different spatial and temporal scales assessed by the two techniques, since our direct
590 comparison between FCS and FRAP measurements yielded similar values of diffusion coefficients.
591 Indeed, a more recent FRAP study also reported higher diffusion coefficients for GFP
592 (Schavemaker, Smigiel, and Poolman 2017).

593 Several proteins in our set showed much lower mobility than expected from their size, and in some
594 cases also clearly subdiffusive behavior. For three selected examples, this deviation could be
595 explained by specific association with other proteins or multiprotein complexes, since disrupting
596 these interactions both increased protein mobility and reduced subdiffusion. This is consistent with
597 theoretical studies suggesting that binding of diffusing molecules to crowders can lead to
598 subdiffusion (Saxton 2007; Guigas and Weiss 2008). Thus, protein-protein interactions may be the
599 main cause of protein subdiffusion in bacterial cytoplasm, although other explanations might hold
600 for subdiffusion of large cytoplasmic particles (Golding and Cox 2004; Lampo et al. 2017; Yu et
601 al. 2018).

602 Unspecific transient interactions might also explain the slightly subdiffusive behavior of sfGFP
603 fusions to proteins from other bacteria in *E. coli* cytoplasm. However, this anomaly was weak and
604 there was overall only little difference between the mobility of these non-native proteins and their
605 similarly-sized *E. coli* homologues, which is in contrast to pronounced differences observed
606 between bacterial and mammalian proteins (Mu et al. 2017). Thus, there is apparently little
607 organism-specific adaptation of freely diffusing proteins to their "bacterial host", with a possible
608 exception of bacteria with extreme pH or ionic strength of the cytoplasm (Schavemaker, Smigiel,
609 and Poolman 2017). This might facilitate horizontal gene transfer among bacteria, by ensuring that
610 their surface properties do not hinder accommodation of proteins in a new host.

611 We further probed how the effective viscous properties of bacterial cytoplasm changed under
612 different physicochemical perturbations, using a subset of proteins that showed fastest diffusion
613 for their molecular mass as reporters of unhindered diffusion. Consistent with the importance of
614 macromolecular crowding and in agreement with previous results (Konopka et al. 2009), protein
615 mobility decreased upon osmotic upshift as cytoplasmic crowding increases. In contrast, the

616 effective cytoplasmic viscosity decreases significantly (~20%) upon treatment with rifampicin that
617 inhibits transcription and thereby reduces the overall macromolecular crowding. This observation
618 is consistent with recent SPT measurements on large cytoplasmic particles (Wlodarski et al. 2020;
619 Rotter et al. 2021), and it agrees well with the relative contribution of RNA to the macromolecular
620 composition of an *E. coli* cell (Cayley et al. 1991) and with the reduction of molecular crowding
621 in rifampicin-treated cells (Wlodarski et al. 2020).

622 Despite multiple effects of environmental temperature on cellular processes, such as the active
623 (nonthermal) stirring of the cytoplasm at higher temperature (Weber, Spakowitz, and Theriot
624 2012), the temperature dependence of the cytoplasmic viscosity in the tested range was similar to
625 that of water and consistent with the Stokes-Einstein relation, decreasing by 20-30% for a
626 temperature increase of 10°C (Huber et al. 2009). Furthermore, the same temperature dependence
627 of protein mobility was observed upon treatment with the protonophore DNP that deenergizes cells
628 by dissipating proton gradient, arguing against general active stirring of cytoplasm in *E. coli* under
629 our experimental conditions. We further observed no dependence of the effective cytoplasmic
630 viscosity on growth temperature, in contrast to the homeostatic adaptation of bacterial membrane
631 fluidity (Sinensky 1974) and of bacterial signaling (Oleksiuk et al. 2011; Almblad et al. 2021) to
632 the growth temperature. Since growth-temperature dependent adaptation of the cytosolic viscosity
633 was recently reported for budding yeast (Persson, Ambati, and Brandman 2020), it is surprising
634 that such compensation apparently does not exist in *E. coli*. One possible explanation for this
635 difference might be a broader range of growth temperatures for budding yeast *Saccharomyces*
636 *cerevisiae* compared to *E. coli,* and a stronger temperature effect on protein diffusion in the yeast
637 cytosol. Of note, here we did not explore protein diffusion in thermally stressed *E. coli* cells, which
638 might have more profound effects on the properties of bacterial cytoplasm as recently shown for
639 *Listeria monocytogenes* (Tran et al. 2021).

640 Finally, we observed that protein mobility was significantly higher in rapidly growing cells. This
641 "fluidizing" effect of growth seems to be primarily due to the biosynthetic processes, likely protein
642 translation, as evidenced by the reduced mobility upon chloramphenicol treatment, or to cell
643 growth itself. The contribution of metabolic activity in presence of nutrients was also significant
644 but weaker, although it might be underestimated since inhibition of protein biosynthesis by
645 chloramphenicol could possibly indirectly reduce metabolic activity. Thus, the observed
646 phenomenon may be different from previously characterized ATP-dependent fluidization of the
647 bacterial cytoplasm that enables mobility of large multiprotein complexes but apparently does not
648 affect free GFP (Montero Llopis et al. 2012; Parry et al. 2014), as also observed for sfGFP and
649 other constructs in our experiments. The interplay between these energy-, metabolism- and growth-
650 dependent effects on diffusional properties of bacterial cytoplasm remains to be investigated.

651 Importantly, we observed that these perturbations to the cytoplasmic protein mobility, including
652 cell growth and changes to the macromolecular crowding and temperature, have proportional
653 effects on differently-sized proteins. These results suggest that - within the tested size range -
654 protein diffusion in *E. coli* cytoplasm remains Brownian under all tested conditions, including
655 growing cells, and effects of these perturbations on protein mobility can be simply accounted for
656 by changes in the cytoplasmic viscosity. We hypothesize that such proportional changes in
657 diffusion of differently-sized proteins might be important to maintain balanced rates of diffusion-
658 limited cellular processes under various environmental conditions.

659

660 # Materials and methods

661 ## Bacterial strains, plasmids and media

662 All strains and plasmids used in this study are listed in Figure 1 – supplementary table 2. All
663 experiments were performed in the *Escherichia coli* strain W3110 (Serra et al. 2013). Genes of
664 interest were amplified by PCR using Q5 polymerase (New England Biosciences) and cloned in
665 frame with sfGFP using Gibson assembly (Gibson et al. 2009) into pTrc99A vector (Amann, Ochs,
666 and Abel 1988), under control of the *trc* promoter inducible by isopropyl ß-D-1-
667 thiogalactopyranoside (IPTG). In all cases sfGFP was fused at the C-terminus of the protein of
668 interest with a GGGGS linker. The stability of the fusion constructs was verified by gel
669 electrophoresis and immunoblotting using an anti-GFP primary antibody (JL-8 monoclonal,
670 Takara). Point mutations were introduced by site-directed mutagenesis (New England
671 Biosciences). The *ΔclpA* strain was generated by transferring the kanamycin resistance cassette
672 from the corresponding mutant in the Keio collection (Baba et al. 2006) by P1 transduction. The
673 cassette was further removed by FLP recombinase carried on the temperature-sensitive plasmid
674 pCP20 (Cherepanov and Wackernagel 1995).

675 *E. coli* cultures were grown in M9 minimal medium (48 mM Na_2HPO_4, 22 mM KH_2PO_4, 8.4 mM
676 NaCl, 18.6 mM NH_4Cl, 2 mM $MgSO_4$, 0.1 mM $CaCl_2$) supplemented with 0.2% casamino acids,
677 20 mM glucose and 100 µg/mL ampicillin for selection. The overnight cultures were diluted to
678 OD_{600} = 0.035 and grown for 3.5 hours at 37°C and 200 rpm shaking. Cultures were treated for
679 additional 45 minutes, under the same temperature and shaking conditions, with 100 µg/mL
680 cephalexin and with 0 - 15 µM IPTG (Figure 1 – supplementary table 1), to induce expression of
681 the fluorescent protein constructs. Where indicated, cultures were further incubated with 200
682 µg/mL rifampicin, DMSO as a mock treatment, 200 µg/mL chloramphenicol or 2 mM DNP for 1
683 hour or with 1 µg/mL A22 for 4 hours under the same temperature and shaking conditions.

684

685 ## Growth curves

686 Measurements of bacterial growth were performed using 96-well plates (Cellstar transparent flat-
687 bottom, Greiner). Overnight cultures were inoculated at an initial OD_{600} of 0.01 in the same
688 medium as used for growth in other experiments. Each well contained 150 µl of culture and the
689 plate was covered with the plastic cover provided by the producer and further sealed with parafilm
690 that prevents evaporation but allows air exchange. Plates were incubated at 37°C with continuous
691 shaking, alternating between 150 s orbital and 150 s linear, in a Tecan Infinite® 200 PRO plate
692 reader.

693

694 ## FCS data acquisition

695 Cells were harvested by centrifugation at 7000g for 3 minutes and washed 3 times in tethering
696 buffer (10 mM K_2HPO_4, 10 mM KH_2PO_4, 1 µM methionine, 10 mM sodium lactate, buffered with
697 NaOH to pH 7). When indicated, 1 mL of chloramphenicol-treated cells were stained for 15
698 minutes with 300 nM SYTOX Orange Nucleic Acid Stain (Invitrogen). The excess of SYTOX
699 Orange was washed in tethering buffer before proceeding with FCS experiments. 2.5 µL of
700 bacterial cells were then spread on a small 1% agarose pad prepared in tethering buffer salts (10
701 mM K_2HPO_4, 10 mM KH_2PO_4 buffered with NaOH to pH 7)**,** unless differently stated. Imaging
702 was performed on Ibidi 2-well µ-Slides (#1.5H, 170 µm ± 5 µm). After the 45 minutes treatment
703 with cephalexin, length of most bacterial cells was in a range of 4-8 µm.

704 FCS measurements were performed on a LSM 880 confocal laser scanning microscope (Carl Zeiss
705 Microscopy) using a C-Apochromat 40×/1.2 water immersion objective selected for FCS. sfGFP

706 was excited with a 488 nm Argon laser (25 mW) and fluorescence emission was collected from
707 490 to 580 nm. SYTOX Orange was excited with a 543 nm laser and fluorescence emission was
708 collected from 553 to 615 nm. In order to avoid partial spectral overlap between the emission
709 spectra of sfGFP and SYTOX Orange, fluorescence emission of sfGFP in the co-staining
710 experiments was collected from 490 to 535 nm. Each sample was equilibrated for at least 20
711 minutes at 25°C (or 35°C when specified), on the stage of the microscope and measurements were
712 taken at the same temperature. FCS measurements were acquired within 60 minutes from the
713 sample preparation. The pinhole was aligned on a daily basis, by maximizing the fluorescence
714 intensity count rate of an Alexa488 (Invitrogen) solution (35 nM) in phosphate-buffered saline
715 (PBS; 137 mM NaCl, 2.7 mM KCl, 8 mM Na_2HPO_4, 1.8 mM KH_2PO_4, pH 7.4). Unless differently
716 stated, all measurements were performed with a pinhole size correspondent to 1 Airy unit, to ensure
717 the optimal gathering of fluorescence signal. The coverslip collar adjustment ring of the water
718 immersion objective was also adjusted daily, maximizing the fluorescence intensity signal and the
719 brightness of Alexa 488. The laser power was adjusted in order to obtain molecular brightness (i.e.
720 photon counts per second per molecule, cpsm) of 10 kcpsm for Alexa 488, using the ZEN software
721 (Carl Zeiss Microscopy). The brightness of Alexa 488 was used as a daily reference to ensure
722 constant laser power and adjusting it using the software-provided laser power percentage whenever
723 necessary (range over the entire set of measurements was 0.11 – 0.18%). Before each measurement
724 session, we acquired three sequential FCS measurements of Alexa488 in PBS, to verify the
725 reproducibility of the confocal volume shape and size. The ratio between axial and lateral beam
726 waist $S = \frac{z_0}{\omega_0}$ = 8.0 ± 0.2 (Avg. ± SEM) was obtained from a Brownian fit of the Alexa 488
727 autocorrelation curves using the ZEN software. For the lateral beam waist, we obtained ω_0 = 0.186
728 ± 0.001 μm (Avg. ± SEM), calculated from the diffusion time τ_D = 20.9 ± 0.11 μs (Avg. ± SEM)

729 obtained from the Brownian fit, being

730 $$D = \frac{\omega_0^2}{4\tau_D} \quad (1)$$

731 and being $D_{Alexa488}$ = 414 μm^2/s at 25°C (Petrov et al. 2006).

732 For the FCS measurements *in vivo*, the laser was positioned at the center of the short length axis
733 and typically 0.8-1 μm from one of the cell poles along the long axis. For each cell, six sequential
734 fluorescence intensity acquisitions of 20 seconds each were performed on the same spot (Figure 1
735 – figure supplement 3). The laser power used for measurements *in vivo* was fixed to a value about
736 7 times lower than for Alexa488 in PBS, in order to reduce photobleaching. Confocal images of
737 the selected cell were routinely acquired before and after the FCS measurement to verify focal (*z*)
738 and positioning (*xy*) stability (see Appendix 1 for additional information on the FCS
739 measurements).

740

741 **FCS data analysis**

742 Due to the small size of bacterial cells, fluorescence intensity traces are affected by photobleaching
743 (Appendix 1). The effect of photobleaching on autocorrelation curves was corrected by detrending
744 the long-time fluorescence decrease of each of the six fluorescence intensity traces using an ImageJ
745 plugin (Jay Unruh, https://research.stowers.org/imagejplugins/index.html, Stowers Institute for
746 Medical Research, USA). The plugin calculates the autocorrelation function (ACF) from each
747 fluorescence intensity trace, correcting it for the photobleaching effect by approximating the
748 decreasing fluorescence intensity trend with a multi-segment line (the number of segments was
749 fixed to two). We obtained almost identical ACFs correcting for photobleaching effects by local
750 averaging (Appendix 1 - figure 3) using the FCS-dedicated software package Fluctuation Analyzer

751 (Wachsmuth et al. 2015). In both cases, ACFs were calculated starting at 2 μs, since at times shorter
752 than 2 μsec, ACFs can be significantly affected by the GaAsp photomultipliers afterpulsing.

753 For each FCS measurement, we fitted all the six ACFs, calculated using the multi-segment
754 detrending method, with a three-dimensional anomalous diffusion model that includes one
755 diffusive component and one blinking component due to the protonation-deprotonation of the
756 chromophore of sfGFP, according to the Equation (2):

757 $$G(\tau) = G_\infty + \frac{1}{N}\left(\frac{1-F_P+F_P e^{-\frac{\tau}{\tau_P}}}{1-F_P}\right)\frac{1}{1+\left(\frac{\tau}{\tau_D}\right)^\alpha\sqrt{1+\frac{1}{S^2}\left(\frac{\tau}{\tau_D}\right)^\alpha}} \quad (2)$$

758 where N is the average number of particles in the confocal volume, F_P is the fraction of particles
759 in the non-fluorescent state, τ_P is the protonation-deprotonation lifetime at pH 7.5, $S = \frac{z_0}{\omega_0}$, the
760 aspect ratio of the confocal volume with z_0 and ω_0 being the axial and lateral beam waists, τ_D is the
761 diffusion time in the confocal volume, α is the anomalous diffusion exponent, and G_∞ is the offset
762 of the autocorrelation function. The protonation-deprotonation lifetime (τ_P) for sfGFP was fixed to
763 25 μs according to FCS measurements for sfGFP in PBS at pH 7.5 (Cotlet et al. 2006). The aspect
764 ratio of the confocal volume was fixed to $S = 8$ in the fittings to be consistent with the experimental
765 calibration (see above). All other parameters were left free. For each FCS measurement, we
766 calculated the average diffusion time τ_D and the average anomalous diffusion exponent α based on
767 the autocorrelation curves of the six sequential fluorescence intensity traces. Importantly, no
768 significant trend in τ_D or α was apparent when comparing the six sequential autocorrelation
769 functions acquired for a given bacterial cell (Appendix 1 - figure 4). Fitting to the anomalous
770 diffusion model was performed using the Levenberg-Marquardt algorithm in the FCS analysis-
771 dedicated software QuickFit 3.0 developed by Jan Wolfgang Krieger and Jörg Langowski

772 (Deutsches Krebsforschungszentrum, Heidelberg, https://github.com/jkriege2/QuickFit3).
773 Identical results were obtained when fitting the data with OriginPro.

774 Alternatively, the autocorrelation functions were fitted by the Ornstein-Uhlenbeck model
775 (Appendix 2) according to Equation (3):

776 $$G(\tau) = G_\infty + \frac{1}{N}\left(\frac{1-F_P+F_P e^{-\frac{\tau}{\tau_P}}}{1-F_P}\right)\left(1+2\frac{\sigma^2}{\omega_0^2}\frac{1-e^{-\frac{1\omega_0^2}{2\sigma^2}\frac{\tau}{\tau_D}}}{1+\frac{1\omega_0^2}{8\sigma^2}}\right)^{-\frac{1}{2}}\left(1+\frac{\tau}{\tau_D}\right)^{-\frac{1}{2}}\left(1+2\frac{\sigma^2}{S^2\omega_0^2}\frac{1-e^{-\frac{1\omega_0^2}{2\sigma^2}\frac{\tau}{\tau_D}}}{1+\frac{1}{8}\frac{S^2\omega_0^2}{\sigma^2}}\right)^{-\frac{1}{2}}$$

777 (3)

778 where S and τ_P were fixed to the same values mentioned for equation (2), ω_0 was fixed to 0.19 and
779 σ was fixed to $d/2$=0.42 µm, being d the typical diameter of an *E. coli* cell (see Ornstein-Uhlenbeck
780 model validation paragraph). Fitting to the Ornstein-Uhlenbeck model was performed with
781 OriginPro.

782

783 FRAP data acquisition and analysis

784 Cells for FRAP experiments were grown and prepared for imaging following the same protocol as
785 for the FCS measurements. Due to the higher sensitivity of FCS at low fluorophore concentrations,
786 several fusion constructs required higher induction by IPTG (Figure 1 – supplementary table 1) to
787 obtain fluorescence intensity suitable for FRAP. The same LSM 880 confocal microscope,
788 including objective and light path was used for FRAP as for the FCS measurements. The bacterial
789 cell was imaged at 40×40 pixels with 30× zoom (pixel size 0.177 µm) with a pixel dwell time of
790 3.15 µs. First, 15 pre-bleaching frames were acquired at 2% laser power, subsequently the
791 photobleaching was performed on a 3×3 pixels area on one cell pole with 100% laser power for a
792 total of 48 ms and 584 post-bleaching frames were acquired to monitor the fluorescence recovery.

793 We observed that the mobile fraction for all constructs was >0.9. FRAP measurements were
794 analyzed using simFRAP (Blumenthal et al. 2015), an ImageJ plugin based on a simulation
795 approach implemented in a fast algorithm, which bypasses the need of using analytical models to
796 interpolate the data. The simFRAP algorithm simulates two-dimensional random walks in each
797 pixel, using the first image acquired after bleaching to define initial and boundary conditions, and
798 it resolves numerically the diffusion equation by iterative simulation. The frame time and pixel size
799 were fixed respectively to 0.018 s and 0.177 μm, and the target cell and the bleached region were
800 defined as ImageJ ROIs (regions of interest). Of note, we used the target cell itself as a reference
801 to compensate for the gradual bleaching during the measurement, as done previously (Kumar,
802 Mommer, and Sourjik 2010). This enabled us to achieve the highest possible temporal resolution,
803 by reducing the acquisition area to a single *E. coli* cell. The FRAP derived diffusion coefficient
804 D_{FRAP} was directly obtained as output of the plugin.

805

806 **Cellular density measurements**

807 Cell cultures were grown following the same protocol as for the FCS and FRAP measurements.
808 Cultures were harvested at 4000g for 5 minutes, and the pellet was resuspended in motility buffer
809 (MB) (10 mM KPO_4, 0.1 mM EDTA, 67 mM NaCl, 0.01% Tween 80). Tween 80 is a surfactant
810 that prevents cell-surface adhesion (Nielsen et al. 2016; Schwarz-Linek et al. 2016). Bacterial
811 suspension was adjusted to a high cell density (OD_{600}=15) by subsequent centrifugation (4000g, 5
812 minutes) and resuspension in a medium containing 20% iodixanol to match the density of MB with
813 that of *E. coli* cell (1.11 g/ml) (Martínez-Salas, Martín, and Vicente 1981). Each sample was then
814 loaded in the chamber of a previously fabricated poly-di-methylsiloxane (PDMS) microfluidic
815 device. The chamber consists of an inlet connected to an outlet by a straight channel of 50 μm

816 height, 1 mm width and 1 cm length. The channel was then sealed with grease to prevent fluid
817 flows. After letting the mixtures reach the steady state in the microfluidic device for 40 minutes,
818 cell sedimentation was visualized by acquiring Z-stack images of the whole microfluidic channel
819 using the same microscopy setup as for the FCS and FRAP measurements (1px = 0.2 μm in X and
820 Y, 1px = 1 μm in Z; field of view = 303.64 x 303.64 x 70 μm^3, 0.35 μs/px exposure). The number
821 of cells in each Z plane was quantified by the connected components labeling algorithm for ImageJ
822 (Legland, Arganda-Carreras, and Andrey 2016). Each experiment was conducted in three technical
823 replicates. Because the height and the tilt of the microfluidic channels slightly varies from sample
824 to sample, the Z position was binned and the mean of the cell fraction over the bins was calculated.

825 The vertical density profiles were fitted to the theoretical expectation for diffusing particles in a
826 buoyant fluid, $n(z) = n_o \exp\left(-\frac{z}{z_o}\right)$, in the range $z = [0.25, 0.8] \times 50$ μm to avoid effects of
827 sample boundaries. The fitted decay length is expected to obey $\frac{1}{z_o} = \frac{\Delta\rho V g}{k_B T}$, with $\Delta\rho$ the difference
828 in density between the cells and the suspending fluid, V the average volume of the cells, $g = 9.81$
829 m^2/s the acceleration of gravity and $k_B T = 4.11$ pN·nm the thermal energy at 25°C. To compute
830 the buoyancy-corrected cell density $\Delta\rho = \frac{k_B T}{V g\, z_o}$, the cell volume was estimated assuming the cells
831 are cylinders closed by hemispherical caps, $V = \pi d^3/6 + (L - d)\pi d^2/4$. For all conditions, the
832 cell diameter d was evaluated on confocal images taken prior to FCS measurement (see Figure 1 –
833 figure supplement 7, Figure 2C and Figure 5 – figure supplement 1), and so was the length of
834 cephalexin treated cells (L = 5.5 ± 0.1 (SEM) μm), cephalexin + A22 treated cells (L = 5.8 ± 0.1
835 (SEM) μm), and untreated cells (L=2.8 ± 0.2 μm). Cell length for 100 mM NaCl, DMSO,
836 rifampicin and chloramphenicol treated cells was kept equal to the one of untreated cells, because
837 cephalexin was not used during culture growth for sedimentation assay for these conditions.

Brownian dynamics simulations

We performed Brownian dynamics simulations of uncorrelated point particles under confinement. The N = 50 fluorescent particles performed a random walk with steps taken from a Gaussian distribution of width $\sqrt{2D\Delta t}$, with D the free diffusion coefficient and $\Delta t = 10^{-6}\ s$ the simulation step. Confinement was imposed by redrawing the random steps that moved out of the confinement volume. Imposing elastic reflections on the walls yielded identical results. The confinement volume was assumed to be a cylinder of diameter d and length (L-d) closed at both ends by hemispheric caps of diameter d, idealizing the shape of *E. coli*. The cell length was fixed to L = 5 μm. The diameter was varied in the range d = [0.7, 1] μm. The collected fluorescence intensity was computed at each time step assuming a Gaussian intensity profile of the laser beam, $I(t) = \sum_{i=1}^{N} I_G(\boldsymbol{r}_i(t) - \boldsymbol{r}_0)$ with $\boldsymbol{r}_i(t)$ the position of particle i, $\boldsymbol{r}_0$ the center of the confocal volume and $I_G\big(\boldsymbol{r} = (x, y, z)\big) = \exp\left(-2\left(\frac{x^2+y^2}{\omega_0^2} + \frac{z^2}{z_0^2}\right)\right)$, with $\omega_0 = 200$ nm and $z_0 = 800$ nm the lateral and axial widths of the confocal volume. The normalized intensity autocorrelation $C(dt) = \frac{\langle I(t+dt)I(t)\rangle}{\langle I(t+dt)\rangle\langle I(t)\rangle} - 1$ is computed for logarithmically spaced lag times dt, to reflect experimental practices. The center of the confocal volume was chosen in the center of the cell along the y and z axes and 1 μm away from the edge of the cell along the longitudinal x axis of the cell, similarly to experimental conditions. The intensity autocorrelation function was finally multiplied by an exponential decay, $\left(1 + 0.1 * \exp - \frac{dt}{\tau_H}\right)/1.1$ with $\tau_H = 25$ μs, to mimic the blinking component due to the protonation-deprotonation process of sfGFP, before fitting with the different models of diffusion. The code used for this simulation is available in GitHub

(https://github.com/croelmiyn/Simulation_FCS_in_Bacteria) and via DOI: 10.5281/zenodo.5940484.

Validation of fitting by the Ornstein-Uhlenbeck model

We first estimated the relation between the width σ of the potential well and the diameter d of the bacteria by fitting the ACF of the Brownian simulations with the OU model, fixing all parameters except σ to their ansatz values. The best fit was obtained for $\sigma \simeq d/2$ over the whole range of tested parameters. To mimic the fit procedure of experimental data and evaluate the accuracy of the diffusion coefficient estimation by the OU model (Figure 2 – figure supplement 3), we then fixed $\sigma = d/2$, and ω_0 and z_0 to their ansatz values, since they are measured independently in experiments, whereas the diffusion coefficient, number of particles N in the confocal volume, fraction of triplet excitation and background noise were taken as free parameters.

Acknowledgements

We thank Lotte Søgaard-Andersen, Martin Thanbichler, Knut Drescher and Andreas Diepold for providing bacterial genomic DNA. We thank Silvia Espada Burriel for the assistance with the cellular density measurements and data analysis. This work was supported by the Max Planck Society.

Competing Interests

The authors declare no competing interests.

References

Agudo-Canalejo, Jaime, Tunrayo Adeleke-Larodo, Pierre Illien, and Ramin Golestanian. 2018. 'Enhanced Diffusion and Chemotaxis at the Nanoscale', *Accounts of Chemical Research*, 51: 2365-72.

Agudo-Canalejo, Jaime, and Ramin Golestanian. 2020. 'Diffusion and steady state distributions of flexible chemotactic enzymes', *The European Physical Journal Special Topics*, 229: 2791-806.

Agudo-Canalejo, Jaime, Pierre Illien, and Ramin Golestanian. 2020. 'Cooperatively enhanced reactivity and "stabilitaxis" of dissociating oligomeric proteins', *Proceedings of the National Academy of Sciences*, 117: 11894.

Almblad, Henrik, Trevor E. Randall, Fanny Liu, Katherine Leblanc, Ryan A. Groves, Weerayuth Kittichotirat, Geoffrey L. Winsor, Nicolas Fournier, Emily Au, Julie Groizeleau, Jacquelyn D. Rich, Yuefei Lou, Elise Granton, Laura K. Jennings, Larissa A. Singletary, Tara M. L. Winstone, Nathan M. Good, Roger E. Bumgarner, Michael F. Hynes, Manu Singh, Maria Silvina Stietz, Fiona S. L. Brinkman, Ayush Kumar, Ann Karen Cornelia Brassinga, Matthew R. Parsek, Boo Shan Tseng, Ian A. Lewis, Bryan G. Yipp, Justin L. MacCallum, and Joe Jonathan Harrison. 2021. 'Bacterial cyclic diguanylate signaling networks sense temperature', *Nature Communications*, 12: 1986.

Amann, E., B. Ochs, and K. J. Abel. 1988. 'Tightly regulated tac promoter vectors useful for the expression of unfused and fused proteins in *Escherichia coli*', *Gene*, 69: 301-15.

Baba, T., T. Ara, M. Hasegawa, Y. Takai, Y. Okumura, M. Baba, K. A. Datsenko, M. Tomita, B. L. Wanner, and H. Mori. 2006. 'Construction of *Escherichia coli* K-12 in-frame, single-gene knockout mutants: the Keio collection', *Molecular Systems Biology*, 2: 2006 0008.

Bakshi, Somenath, Benjamin P Bratton, and James C Weisshaar. 2011. 'Subdiffraction-Limit Study of Kaede Diffusion and Spatial Distribution in Live *Escherichia coli*', *Biophysical Journal*, 101: 2535-44.

907 Bakshi, Somenath, Heejun Choi, Jagannath Mondal, and James C. Weisshaar. 2014. 'Time-
908 dependent effects of transcription- and translation-halting drugs on the spatial
909 distributions of the *Escherichia coli* chromosome and ribosomes', *Molecular*
910 *Microbiology*, 94: 871-87.

911 Balbo, Jessica, Paolo Mereghetti, Dirk-Peter Herten, and Rebecca C. Wade. 2013. 'The shape of
912 protein crowders is a major determinant of protein diffusion', *Biophysical Journal*, 104:
913 1576-84.

914 Banks, Daniel S., and Cécile Fradin. 2005. 'Anomalous Diffusion of Proteins Due to Molecular
915 Crowding', *Biophysical Journal*, 89: 2960-71.

916 Blumenthal, D., L. Goldstien, M. Edidin, and L. A. Gheber. 2015. 'Universal Approach to FRAP
917 Analysis of Arbitrary Bleaching Patterns', *Scientific Reports*, 5: 11655.

918 Cayley, Scott, Barbara A. Lewis, Harry J. Guttman, and M. Thomas Record. 1991.
919 'Characterization of the cytoplasm of *Escherichia coli* K-12 as a function of external
920 osmolarity: Implications for protein-DNA interactions in vivo', *Journal of Molecular*
921 *Biology*, 222: 281-300.

922 Cherepanov, Peter P., and Wilfried Wackernagel. 1995. 'Gene disruption in *Escherichia coli*:
923 TcR and KmR cassettes with the option of Flp-catalyzed excision of the antibiotic-
924 resistance determinant', *Gene*, 158: 9-14.

925 Cluzel, Philippe, Michael Surette, and Stanislas Leibler. 2000. 'An Ultrasensitive Bacterial Motor
926 Revealed by Monitoring Signaling Proteins in Single Cells', *Science*, 287: 1652-55.

927 Cotlet, M., P. M. Goodwin, G. S. Waldo, and J. H. Werner. 2006. 'A comparison of the
928 fluorescence dynamics of single molecules of a green fluorescent protein: one- versus
929 two-photon excitation', *Chemphyschem*, 7: 250-60.

930 Di Rienzo, Carmine, Vincenzo Piazza, Enrico Gratton, Fabio Beltram, and Francesco Cardarelli.
931 2014. 'Probing short-range protein Brownian motion in the cytoplasm of living cells',
932 *Nature Communications*, 5: 5891.

933 Diepold, A., E. Sezgin, M. Huseyin, T. Mortimer, C. Eggeling, and J. P. Armitage. 2017. 'A
934 dynamic and adaptive network of cytosolic interactions governs protein export by the
935 T3SS injectisome', *Nature Communications*, 8: 15940.

936 Dix, James A., and A. S. Verkman. 2008. 'Crowding Effects on Diffusion in Solutions and Cells',
937 *Annual Review of Biophysics*, 37: 247-63.

938 Einstein, Albert 1906. 'On the theory of the Brownian movement', *Annalen der Physik*, 19: 371-
939 81.

940 Elowitz Michael, B., G. Surette Michael, Pierre-Etienne Wolf, B. Stock Jeffry, and Stanislas
941 Leibler. 1999. 'Protein Mobility in the Cytoplasm of *Escherichia coli*', *Journal of*
942 *Bacteriology*, 181: 197-203.

943 Elson, E. L. 2011. 'Fluorescence correlation spectroscopy: past, present, future', *Biophysical*
944 *Journal*, 101: 2855-70.

945 Enderlein, Jörg. 2012. 'Polymer Dynamics, Fluorescence Correlation Spectroscopy, and the
946 Limits of Optical Resolution', *Physical Review Letters*, 108: 108101.

947 Enderlein, Jörg, Ingo Gregor, Digambara Patra, Thomas Dertinger, and U. Benjamin Kaupp.
948 2005. 'Performance of Fluorescence Correlation Spectroscopy for Measuring Diffusion
949 and Concentration', *Chemphyschem*, 6: 2324-36.

950 English, Brian P., Vasili Hauryliuk, Arash Sanamrad, Stoyan Tankov, Nynke H. Dekker, and
951 Johan Elf. 2011. 'Single-molecule investigations of the stringent response machinery in
952 living bacterial cells', *Proceedings of the National Academy of Sciences of the United*
953 *States of America*, 108: E365-E73.

954 Enright, Matthew B., and David M. Leitner. 2005. 'Mass fractal dimension and the compactness
955 of proteins', *Physical Review E*, 71: 011912.

956 Etoc, Fred, Elie Balloul, Chiara Vicario, Davide Normanno, Domenik Liße, Assa Sittner, Jacob
957 Piehler, Maxime Dahan, and Mathieu Coppey. 2018. 'Non-specific interactions govern

958 cytosolic diffusion of nanosized objects in mammalian cells', *Nature Materials*, 17: 740-
959 46.

960 Genevaux, P., C. Georgopoulos, and W. L. Kelley. 2007. 'The Hsp70 chaperone machines of
961 *Escherichia coli*: a paradigm for the repartition of chaperone functions', *Molecular*
962 *Microbiology*, 66: 840-57.

963 Gennerich, Arne, and Detlev Schild. 2000. 'Fluorescence Correlation Spectroscopy in Small
964 Cytosolic Compartments Depends Critically on the Diffusion Model Used', *Biophysical*
965 *Journal*, 79: 3294-306.

966 Gibson, D. G., L. Young, R. Y. Chuang, J. C. Venter, C. A. Hutchison, 3rd, and H. O. Smith.
967 2009. 'Enzymatic assembly of DNA molecules up to several hundred kilobases', *Nature*
968 *Methods*, 6: 343-5.

969 Goins, Aron B., Hugo Sanabria, and M. Neal Waxham. 2008. 'Macromolecular crowding and
970 size effects on probe microviscosity', *Biophysical Journal*, 95: 5362-73.

971 Golding, Ido, and Edward C. Cox. 2004. 'RNA dynamics in live *Escherichia coli* cells',
972 *Proceedings of the National Academy of Sciences of the United States of America*, 101:
973 11310.

974 Golestanian, Ramin. 2015. 'Enhanced Diffusion of Enzymes that Catalyze Exothermic Reactions',
975 *Physical Review Letters*, 115: 108102.

976 Guigas, Gernot, and Matthias Weiss. 2008. 'Sampling the Cell with Anomalous Diffusion—The
977 Discovery of Slowness', *Biophysical Journal*, 94: 90-94.

978 Huber, M. L., R. A. Perkins, A. Laesecke, D. G. Friend, J. V. Sengers, M. J. Assael, I. N. Metaxa,
979 E. Vogel, R. Mareš, and K. Miyagawa. 2009. 'New International Formulation for the
980 Viscosity of H2O', *Journal of Physical and Chemical Reference Data*, 38: 101-25.

981 Humbard, M. A., S. Surkov, G. M. De Donatis, L. M. Jenkins, and M. R. Maurizi. 2013. 'The N-
982 degradome of *Escherichia coli*: limited proteolysis in vivo generates a large pool of
983 proteins bearing N-degrons', *The Journal of Biological Chemistry*, 288: 28913-24.

984 Jiang, Yanfei, Bingxian Xu, Artem Melnykov, Guy M. Genin, and Elliot L. Elson. 2020.
985 'Fluorescence Correlation Spectroscopy and Photon Counting Histograms in Finite,
986 Bounded Domains', *Biophysical Journal*, 119: 265-73.

987 Joyner, Ryan P., Jeffrey H. Tang, Jonne Helenius, Elisa Dultz, Christiane Brune, Liam J. Holt,
988 Sebastien Huet, Daniel J. Müller, and Karsten Weis. 2016. 'A glucose-starvation response
989 regulates the diffusion of macromolecules', *Elife*, 5: e09376.

990 Kalwarczyk, Tomasz, Marcin Tabaka, and Robert Holyst. 2012. 'Biologistics--diffusion
991 coefficients for complete proteome of *Escherichia coli*', *Bioinformatics (Oxford,*
992 *England)*, 28: 2971-78.

993 Kapanidis, A. N., S. Uphoff, and M. Stracy. 2018. 'Understanding Protein Mobility in Bacteria by
994 Tracking Single Molecules', *Journal of Molecular Biology*, 430: 4443-55.

995 Klumpp, Stefan, Matthew Scott, Steen Pedersen, and Terence Hwa. 2013. 'Molecular crowding
996 limits translation and cell growth', *Proceedings of the National Academy of Sciences*, 110:
997 16754.

998 Konopka, M. C., I. A. Shkel, S. Cayley, M. T. Record, and J. C. Weisshaar. 2006. 'Crowding and
999 confinement effects on protein diffusion in vivo', *Journal of Bacteriology*, 188: 6115-23.

1000 Konopka, M. C., K. A. Sochacki, B. P. Bratton, I. A. Shkel, M. T. Record, and J. C. Weisshaar.
1001 2009. 'Cytoplasmic protein mobility in osmotically stressed *Escherichia coli*', *Journal of*
1002 *Bacteriology*, 191: 231-7.

1003 Kumar, M., M. S. Mommer, and V. Sourjik. 2010. 'Mobility of cytoplasmic, membrane, and
1004 DNA-binding proteins in *Escherichia coli*', *Biophysical Journal*, 98: 552-9.

1005 Kumar, Mohit, and Victor Sourjik. 2012. 'Physical map and dynamics of the chaperone network
1006 in *Escherichia coli*', *Molecular Microbiology*, 84: 736-47.

1007 Lampo, Thomas J., Stella Stylianidou, Mikael P. Backlund, Paul A. Wiggins, and Andrew J.
1008 Spakowitz. 2017. 'Cytoplasmic RNA-Protein Particles Exhibit Non-Gaussian
1009 Subdiffusive Behavior', *Biophysical Journal*, 112: 532-42.

1010 Langevin, Paul. 1908. 'Sur la théorie du mouvement brownien', *Comptes-rendus de l'Académie*
1011 *des sciences*, 146: 530-33.

1012 Legland, David, Ignacio Arganda-Carreras, and Philippe Andrey. 2016. 'MorphoLibJ: integrated
1013 library and plugins for mathematical morphology with ImageJ', *Bioinformatics (Oxford,*
1014 *England)*, 32: 3532-34.

1015 Liu, B., Z. Hasrat, B. Poolman, and A. J. Boersma. 2019. 'Decreased Effective Macromolecular
1016 Crowding in *Escherichia coli* Adapted to Hyperosmotic Stress', *Journal of Bacteriology*,
1017 201.

1018 Loren, N., J. Hagman, J. K. Jonasson, H. Deschout, D. Bernin, F. Cella-Zanacchi, A. Diaspro, J.
1019 G. McNally, M. Ameloot, N. Smisdom, M. Nyden, A. M. Hermansson, M. Rudemo, and
1020 K. Braeckmans. 2015. 'Fluorescence recovery after photobleaching in material and life
1021 sciences: putting theory into practice', *Quarterly Reviews of Biophysics*, 48: 323-87.

1022 Luby-Phelps, Katherine. 1999. 'Cytoarchitecture and Physical Properties of Cytoplasm: Volume,
1023 Viscosity, Diffusion, Intracellular Surface Area.' in Harry Walter, Donald E. Brooks and
1024 Paul A. Srere (eds.), *International Review of Cytology* (Academic Press).

1025 Macháň, Radek, Yong Hwee Foo, and Thorsten Wohland. 2016. 'On the Equivalence of FCS and
1026 FRAP: Simultaneous Lipid Membrane Measurements', *Biophysical Journal*, 111: 152-61.

1027 Martínez-Salas, E., J. A. Martín, and M. Vicente. 1981. 'Relationship of Escherichia coli density
1028 to growth rate and cell age', *J Bacteriol*, 147: 97-100.

1029 Mayer, Matthias P., Stefan Rüdiger, and Bernd Bukau. 2000. 'Molecular Basis for Interactions of
1030 the DnaK Chaperone with Substrates', *Biological Chemistry*, 381: 877-85.

1031 Meacci, G., J. Ries, E. Fischer-Friedrich, N. Kahya, P. Schwille, and K. Kruse. 2006. 'Mobility of
1032 Min-proteins in *Escherichia coli* measured by fluorescence correlation spectroscopy',
1033 *Physical Biology*, 3: 255-63.

1034 Mika, J. T., G. van den Bogaart, L. Veenhoff, V. Krasnikov, and B. Poolman. 2010. 'Molecular
1035 sieving properties of the cytoplasm of *Escherichia coli* and consequences of osmotic
1036 stress', *Molecular Microbiology*, 77: 200-7.

1037 Mika, Jacek T., and Bert Poolman. 2011. 'Macromolecule diffusion and confinement in
1038 prokaryotic cells', *Current Opinion in Biotechnology*, 22: 117-26.

1039 Montero Llopis, Paula, Oleksii Sliusarenko, Jennifer Heinritz, and Christine Jacobs-Wagner.
1040 2012. '*In vivo* biochemistry in bacterial cells using FRAP: insight into the translation
1041 cycle', *Biophysical Journal*, 103: 1848-59.

1042 Mu, Xin, Seongil Choi, Lisa Lang, David Mowray, Nikolay V. Dokholyan, Jens Danielsson, and
1043 Mikael Oliveberg. 2017. 'Physicochemical code for quinary protein interactions in
1044 *Escherichia coli*', *Proceedings of the National Academy of Sciences*, 114: E4556.

1045 Mullineaux, C. W., A. Nenninger, N. Ray, and C. Robinson. 2006. 'Diffusion of green
1046 fluorescent protein in three cell environments in *Escherichia coli*', *Journal of*
1047 *Bacteriology*, 188: 3442-8.

1048 Muramatsu, N., and A. P. Minton. 1988. 'Tracer diffusion of globular proteins in concentrated
1049 protein solutions', *Proceedings of the National Academy of Sciences of the United States*
1050 *of America*, 85: 2984-88.

1051 Nenninger, A., G. Mastroianni, and C. W. Mullineaux. 2010. 'Size dependence of protein
1052 diffusion in the cytoplasm of *Escherichia coli*', *Journal of Bacteriology*, 192: 4535-40.

1053 Nielsen, Christina K., Jørgen Kjems, Tina Mygind, Torben Snabe, and Rikke L. Meyer. 2016.
1054 'Effects of Tween 80 on Growth and Biofilm Formation in Laboratory Media', *Frontiers*
1055 *in Microbiology*, 7.

1056 Oldewurtel Enno, R., Yuki Kitahara, and Sven van Teeffelen. 2021. 'Robust surface-to-mass
1057 coupling and turgor-dependent cell width determine bacterial dry-mass density',
1058 *Proceedings of the National Academy of Sciences*, 118: e2021416118.

1059 Oleksiuk, O., V. Jakovljevic, N. Vladimirov, R. Carvalho, E. Paster, W. S. Ryu, Y. Meir, N. S.
1060 Wingreen, M. Kollmann, and V. Sourjik. 2011. 'Thermal robustness of signaling in
1061 bacterial chemotaxis', *Cell*, 145: 312-21.

1062 Ouzounov, N., J. P. Nguyen, B. P. Bratton, D. Jacobowitz, Z. Gitai, and J. W. Shaevitz. 2016.
1063 'MreB Orientation Correlates with Cell Diameter in *Escherichia coli*', *Biophysical*
1064 *Journal*, 111: 1035-43.

1065 Parry, B. R., I. V. Surovtsev, M. T. Cabeen, C. S. O'Hern, E. R. Dufresne, and C. Jacobs-Wagner.
1066 2014. 'The bacterial cytoplasm has glass-like properties and is fluidized by metabolic
1067 activity', *Cell*, 156: 183-94.

1068 Pédelacq, Jean-Denis, Stéphanie Cabantous, Timothy Tran, Thomas C. Terwilliger, and Geoffrey
1069 S. Waldo. 2006. 'Engineering and characterization of a superfolder green fluorescent
1070 protein', *Nature Biotechnology*, 24: 79-88.

1071 Perrin, Jean. 1909. 'Mouvement brownien et réalité moléculaire', *Annales de chimie et de*
1072 *physique*.

1073 Persson, Laura B., Vardhaan S. Ambati, and Onn Brandman. 2020. 'Cellular Control of Viscosity
1074 Counters Changes in Temperature and Energy Availability', *Cell*, 183: 1572-85.e16.

1075 Petrov, E. P., T. Ohrt, R. G. Winkler, and P. Schwille. 2006. 'Diffusion and segmental dynamics
1076 of double-stranded DNA', *Physical Review Letters*, 97: 258101.

1077 Potma, Eric O., Wim P. de Boeij, Leonard Bosgraaf, Jeroen Roelofs, Peter J. M. van Haastert,
1078 and Douwe A. Wiersma. 2001. 'Reduced Protein Diffusion Rate by Cytoskeleton in
1079 Vegetative and Polarized Dictyostelium Cells', *Biophysical Journal*, 81: 2010-19.

1080 Rivas, Germán, and Allen P. Minton. 2016. 'Macromolecular Crowding *In Vitro*, *In Vivo*, and In
1081 Between', *Trends in Biochemical Sciences*, 41: 970-81.

1082 Rocha, J., J. Corbitt, T. Yan, C. Richardson, and A. Gahlmann. 2019. 'Resolving Cytosolic
1083 Diffusive States in Bacteria by Single-Molecule Tracking', *Biophysical Journal*, 116:
1084 1970-83.

1085 Roman-Hernandez, G., J. Y. Hou, R. A. Grant, R. T. Sauer, and T. A. Baker. 2011. 'The ClpS
1086 adaptor mediates staged delivery of N-end rule substrates to the AAA+ ClpAP protease',
1087 *Molecular Cell*, 43: 217-28.

1088 Rotter, D. A. O., C. Heger, L. M. Oviedo-Bocanegra, and P. L. Graumann. 2021. 'Transcription-
1089 dependent confined diffusion of enzymes within subcellular spaces of the bacterial
1090 cytoplasm', *BMC Biology*, 19: 183.

1091 Sabri, Adal, Xinran Xu, Diego Krapf, and Matthias Weiss. 2020. 'Elucidating the Origin of
1092 Heterogeneous Anomalous Diffusion in the Cytoplasm of Mammalian Cells', *Physical*
1093 *Review Letters*, 125: 058101.

1094 Sanamrad, A., F. Persson, E. G. Lundius, D. Fange, A. H. Gynna, and J. Elf. 2014. 'Single-
1095 particle tracking reveals that free ribosomal subunits are not excluded from the
1096 *Escherichia coli* nucleoid', *Proceedings of the National Academy of Sciences of the*
1097 *United States of America*, 111: 11413-8.

1098 Sandikci, A., F. Gloge, M. Martinez, M. P. Mayer, R. Wade, B. Bukau, and G. Kramer. 2013.
1099 'Dynamic enzyme docking to the ribosome coordinates N-terminal processing with
1100 polypeptide folding', *Nature Structural & Molecular Biology*, 20: 843-50.

1101 Saxton, M. J. 1996. 'Anomalous diffusion due to binding: a Monte Carlo study', *Biophysical*
1102 *Journal*, 70: 1250-62.

1103 Saxton, Michael J. 2007. 'A Biological Interpretation of Transient Anomalous Subdiffusion. I.
1104 Qualitative Model', *Biophysical Journal*, 92: 1178-91.

1105 Schavemaker, P. E., W. M. Smigiel, and B. Poolman. 2017. 'Ribosome surface properties may
1106 impose limits on the nature of the cytoplasmic proteome', *Elife*, 6.

1107 Schavemaker, Paul E., Arnold J. Boersma, and Bert Poolman. 2018. 'How Important Is Protein
1108 Diffusion in Prokaryotes?', *Frontiers in Molecular Biosciences*, 5: 93.

1109 Schwartz, Russell, Claire S. Ting, and Jonathan King. 2001. 'Whole Proteome pI Values
1110 Correlate with Subcellular Localizations of Proteins for Organisms within the Three
1111 Domains of Life', *Genome Research*, 11: 703-09.

1112 Schwarz-Linek, Jana, Jochen Arlt, Alys Jepson, Angela Dawson, Teun Vissers, Dario Miroli,
1113 Teuta Pilizota, Vincent A. Martinez, and Wilson C. K. Poon. 2016. 'Escherichia coli as a
1114 model active colloid: A practical introduction', *Colloids and Surfaces B: Biointerfaces*,
1115 137: 2-16.

1116 Serra, D. O., A. M. Richter, G. Klauck, F. Mika, and R. Hengge. 2013. 'Microanatomy at cellular
1117 resolution and spatial order of physiological differentiation in a bacterial biofilm', *mBio*,
1118 4: e00103-13.

1119 Sinensky, M. 1974. 'Homeoviscous adaptation--a homeostatic process that regulates the viscosity
1120 of membrane lipids in *Escherichia coli*', *Proceedings of the National Academy of Sciences*
1121 *of the United States of America*, 71: 522-25.

1122 Smilgies, Detlef- M., and Ewa Folta-Stogniew. 2015. 'Molecular weight-gyration radius relation
1123 of globular proteins: a comparison of light scattering, small-angle X-ray scattering and
1124 structure-based data', *Journal of applied crystallography*, 48: 1604-06.

1125 Solbiati, José, Anne Chapman-Smith, Judith L. Miller, Charles G. Miller, and John E. Cronan.
1126 1999. 'Processing of the N termini of nascent polypeptide chains requires deformylation
1127 prior to methionine removal', *Journal of Molecular Biology*, 290: 607-14.

1128 Spitzer, Jan, and Bert Poolman. 2013. 'How crowded is the prokaryotic cytoplasm?', *FEBS*
1129 *Letters*, 587: 2094-98.

1130 Stasevich, Timothy J., Florian Mueller, Ariel Michelman-Ribeiro, Tilman Rosales, Jay R.
1131 Knutson, and James G. McNally. 2010. 'Cross-validating FRAP and FCS to quantify the
1132 impact of photobleaching on in vivo binding estimates', *Biophysical Journal*, 99: 3093-
1133 101.

1134 Stracy, M., J. Schweizer, D. J. Sherratt, A. N. Kapanidis, S. Uphoff, and C. Lesterlin. 2021.
1135 'Transient non-specific DNA binding dominates the target search of bacterial DNA-
1136 binding proteins', *Molecular Cell*, 81: 1499-514 e6.

1137 Swaminathan, R., C. P. Hoang, and A. S. Verkman. 1997. 'Photobleaching recovery and
1138 anisotropy decay of green fluorescent protein GFP-S65T in solution and cells:
1139 cytoplasmic viscosity probed by green fluorescent protein translational and rotational
1140 diffusion', *Biophysical Journal*, 72: 1900-07.

1141 Tabaka, Marcin, Tomasz Kalwarczyk, Jedrzej Szymanski, Sen Hou, and Robert Holyst. 2014.
1142 'The effect of macromolecular crowding on mobility of biomolecules, association
1143 kinetics, and gene expression in living cells', *Frontiers in Physics*, 2.

1144 Tran, Buu Minh, Haritha Prabha, Aditya Iyer, Conor O'Byrne, Tjakko Abee, and Bert Poolman.
1145 2021. 'Measurement of Protein Mobility in *Listeria monocytogenes* Reveals a Unique
1146 Tolerance to Osmotic Stress and Temperature Dependence of Diffusion', *Frontiers in*
1147 *Microbiology*, 12.

1148 Tyn, Myo T., and Todd W. Gusek. 1990. 'Prediction of diffusion coefficients of proteins',
1149 *Biotechnology and Bioengineering*, 35: 327-38.

1150 van den Berg, Jonas, Arnold J. Boersma, and Bert Poolman. 2017. 'Microorganisms maintain
1151 crowding homeostasis', *Nature Reviews Microbiology*, 15: 309-18.

1152 von Bülow, Sören, Marc Siggel, Max Linke, and Gerhard Hummer. 2019. 'Dynamic cluster
1153 formation determines viscosity and diffusion in dense protein solutions', *Proceedings of*
1154 *the National Academy of Sciences*, 116: 9843-52.

1155 Wachsmuth, M., C. Conrad, J. Bulkescher, B. Koch, R. Mahen, M. Isokane, R. Pepperkok, and J.
1156 Ellenberg. 2015. 'High-throughput fluorescence correlation spectroscopy enables analysis
1157 of proteome dynamics in living cells', *Nature Biotechnology*, 33: 384-9.

1158 Weber, Stephanie, C., Andrew Spakowitz, J., and Julie Theriot, A. 2012. 'Nonthermal ATP-
1159 dependent fluctuations contribute to the in vivo motion of chromosomal loci',
1160 *Proceedings of the National Academy of Sciences*, 109: 7338-43.

1161 Wlodarski, Michal, Leonardo Mancini, Bianca Raciti, Bianca Sclavi, Marco Cosentino
1162 Lagomarsino, and Pietro Cicuta. 2020. 'Cytosolic Crowding Drives the Dynamics of Both
1163 Genome and Cytosol in Escherichia coli Challenged with Sub-lethal Antibiotic
1164 Treatments', *iScience*, 23: 101560.

1165 Yu, Shi, Julian Sheats, Pietro Cicuta, Bianca Sclavi, Marco Cosentino Lagomarsino, and Kevin
1166 D. Dorfman. 2018. 'Subdiffusion of loci and cytoplasmic particles are different in
1167 compressed Escherichia coli cells', *Communications Biology*, 1: 176.

1168 Zhang, Yifei, and Henry Hess. 2019. 'Enhanced Diffusion of Catalytically Active Enzymes', *ACS*
1169 *Central Science*, 5: 939-48.

1170 Zimmerman, Steven B., and Stefan O. Trach. 1991. 'Estimation of macromolecule concentrations
1171 and excluded volume effects for the cytoplasm of *Escherichia coli*', *Journal of Molecular*
1172 *Biology*, 222: 599-620.

1173

1174